



SATHYABAMA

INSTITUTE OF SCIENCE AND TECHNOLOGY
(DEEMED TO BE UNIVERSITY)

Accredited "A" Grade by NAAC | 12B Status by UGC | Approved by AICTE

www.sathyabama.ac.in

SCHOOL OF MECHANICAL ENGINEERING
DEPARTMENT OF AERONAUTICAL ENGINEERING

UNIT – I - ELEMENTS OF HELICOPTER AERODYNAMICS – SAE1608

I.INTRODUCTION

Principles of Flight

A helicopter is a heavier than air flying machine that has a lifting force created by a main rotor according to aerodynamic principles.

The basic components of a helicopter are as follows

- **Main rotor.** Put in motion by the power plant (engine).
- **Fuselage.** Intended for accommodation of crew, passengers, equipment and cargo.
- **Landing gear,** that is, arrangement intended for movement over the ground /6 or for parking.
- **Tail rotor.** Provides directional equilibrium and directional control of the helicopter.
- **Propulsion system** which sets in motion the lifting and tail rotors and auxiliary systems.
- **Transmission transfers** the torque from the power plant to the main and tail rotors.

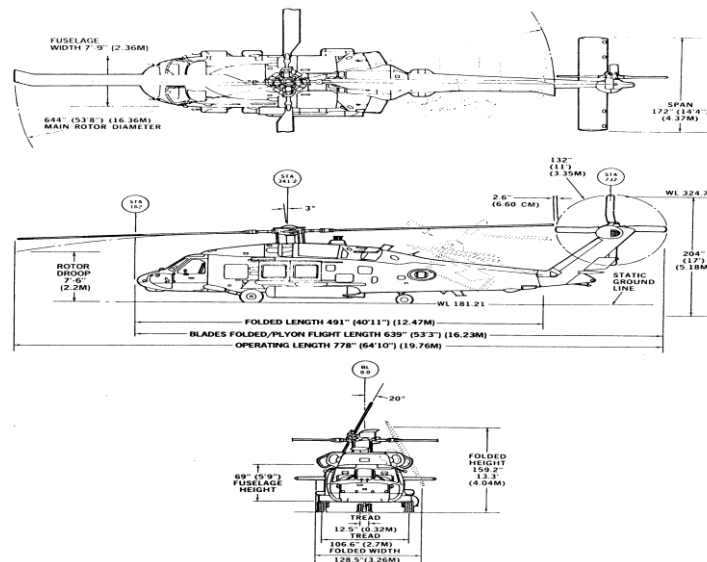


Fig.1

- Flight is possible for a flying machine if there is a lifting force counterbalancing its weight.
- The lifting force of the helicopter originates at the main rotor. By the rotation of the main rotor in the air a thrust force is developed perpendicular to the plane of rotor rotation.
- If the main rotor rotates in the horizontal plane, then its thrust force T is directed vertically upwards (Figure 2), that is, vertical flight is possible.

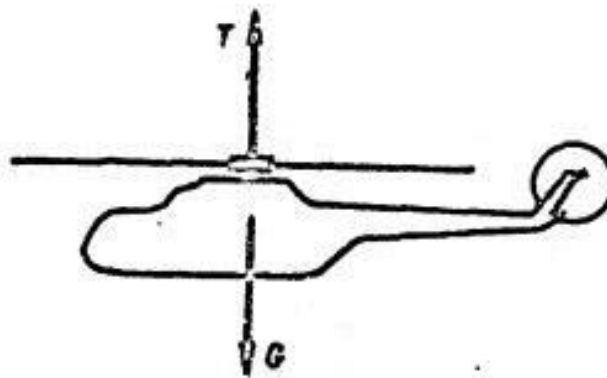


Figure 2: Vertical Flight

- The characteristics of the flight depend on the correlation between the thrust force of the main rotor and the weight of the helicopter.
- If the thrust force equals the weight of the helicopter, then it will remain motionless in the air.
- If, though, the thrust force is greater than the weight, then the helicopter will pass from being motionless into a vertical climb.
- If the thrust force is less than the weight, a vertical descent will result.
- The plane of rotation of the main rotor with respect to the ground can be inclined in any direction (Figure 3).
- In this case the rotor will fulfill a two-fold function; its vertical component Y will be the lift force and the horizontal component P -the propulsive force.
- Under the influence of this force the helicopter moves forward in flight

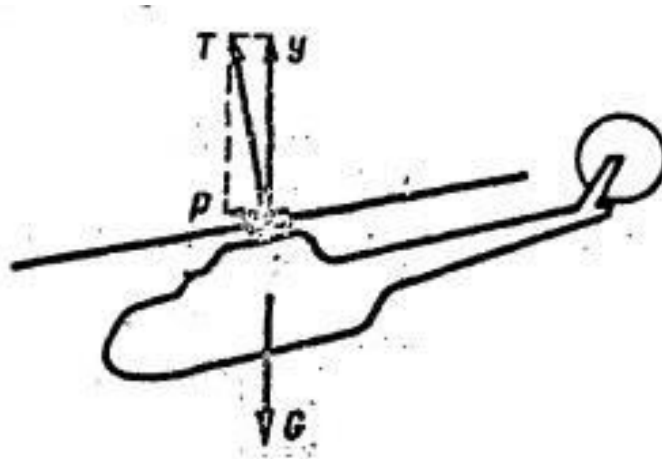


Figure 3: Horizontal flight forwards

- If the plane of the main rotor is inclined backwards, the helicopter will move backwards. (Figure 4).
- The inclination of the plane of rotation to the right or to the left causes motion of the helicopter in the corresponding direction.

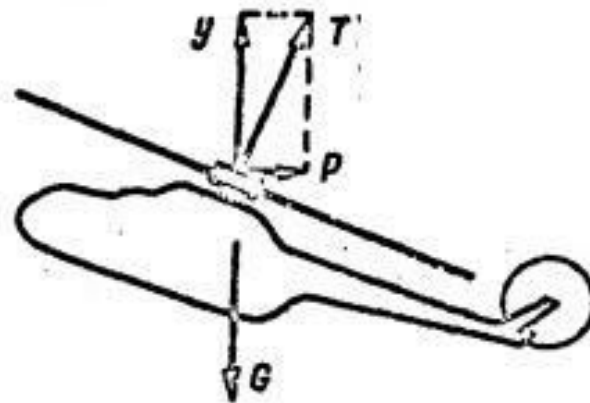


Figure 4: Horizontal flight backwards

II. CLASSIFICATION OF HELICOPTER

The basic classification of helicopter types is that of the number of main rotors and their disposition.

According to the number of main rotors, it is possible to classify helicopters as

- Single Rotor,
- Dual Rotor and
- Multirotor Types.



Figure 5.

Single rotor helicopters

- Single rotor helicopters appear in many varieties.
- Helicopters of the single rotor scheme have a main rotor, mounted on the main fuselage and a tail rotor mounted on the tail structure (see Figure 6).
- This arrangement, which was developed by B. N. Yur'yev in 1911, provides a name for one classification.



Figure 6

- The basic merit of single rotor helicopters is the simplicity of construction and the control system.
- The class of single rotor helicopters includes the very light helicopters (flight weight about 500 kgf), and very heavy helicopters (flight weight greater than 40 tons).
- Some of the deficiencies of the single rotor helicopter are:
 - ✓ Large fuselage length;
 - ✓ A significant loss of power due to the tail rotor drive train (7 - 10% of the full power of the engine);
 - ✓ A limited range of permissible centring;
 - ✓ A higher level of vibration (the long transmission shafts, extending into the tail structure, are additional sources of spring oscillations).

Dual rotor helicopters

- Dual rotor helicopters appear in several arrangements. Rotors arranged in tandem; this is the most prevalent arrangement (Figure 6a);

- Rotors in a transverse arrangement (Figure 5b);
- A cross connected rotor scheme (Figure 5c);
- A coaxial rotor arrangement (Figure 5d).

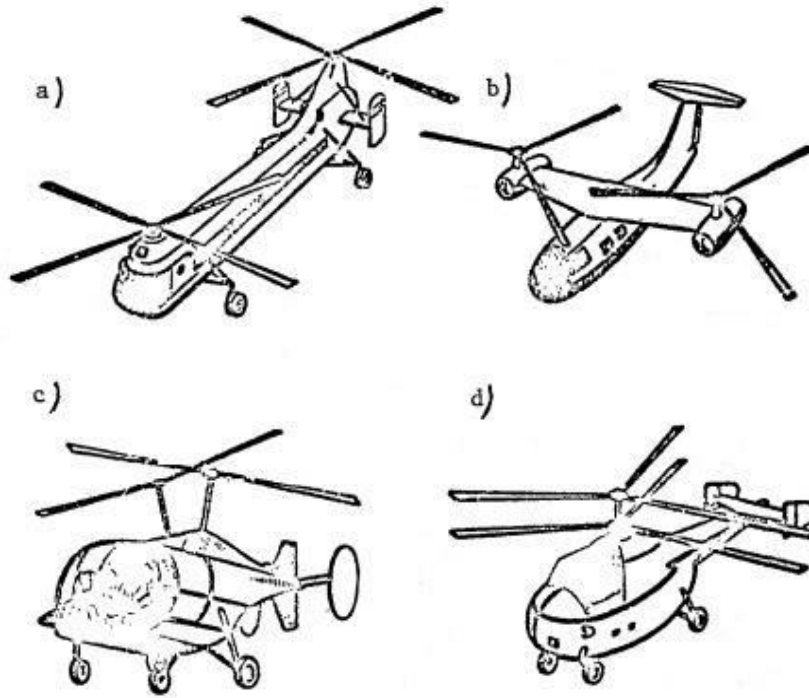


Figure6: Dual Rotor helicopters

The basic merits of helicopters with a tandem rotor arrangement are:

- Wider range of permissible centering;
- Large fuselage volume;
- which allows it to contain large-sized loads;
- Increased longitudinal stability; Large weight coefficient.
- Helicopters with a tandem arrangement of rotors can have one or two engines, which are located in the forward or aft parts of the fuselage.
- These helicopters have the following serious deficiencies:
 - ✓ A complicated system of transmission and control;
 - ✓ Adverse mutual interaction between the main rotors which causes, in addition, a loss of power;
 - ✓ Complicated landing techniques are required in the autorotation regime of main rotors.

The following advantages are attributed to helicopters with a transverse arrangement of rotors :

- ✓ Convenient utilization of all parts of the fuselage for crew and passengers, since the engines are located outside the fuselage;
- ✓ Absence of harmful interaction of one rotor with the other;
- ✓ Higher lateral stability and controllability of the helicopter;
- ✓ The presence of an auxiliary wing, where the engines and main rotors are located, allows the helicopter to develop a high speed.

Deficiencies of these helicopters are as follows:

- A complicated system of control and transmission;
- An increase in size and structure weight due to the presence of the auxiliary wing.
- Dual rotor helicopters with cross connected rotors have a considerable advantage over helicopters with transverse rotors;
- they do not have an auxiliary wing, which reduces the size and structure weight.
- But, at the same time, with these advantages there is a deficiency, -a complicated transmission and control system.

Coaxial rotors Helicopter

- The basic advantage of dual rotor helicopters with coaxial rotors is their small size.
- Their disadvantages: Complicated structure; Deficient directional stability;
- Danger of collision of the rotor blades;
- Considerable vibration.

In the Soviet Union, there are only light helicopters with this rotor arrangement. Multi-rotor helicopters are not widely used in view of their complex construction.

In all dual-rotor helicopters, the main rotors rotate in opposite directions. In this way the mutual reactive moments are balanced, and the necessity of having a tail rotor is eliminated. Thus the power loss from the engine is reduced.

The Main Rotor

The lifting force is produced by the rotors. As they spin they cut into the air and produce lift. Each blade produces an equal share of the lifting force.

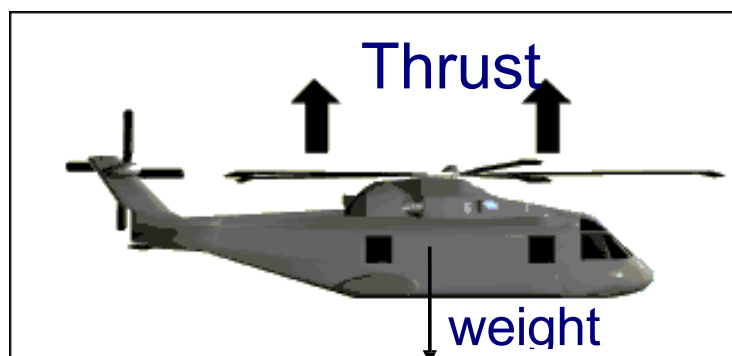


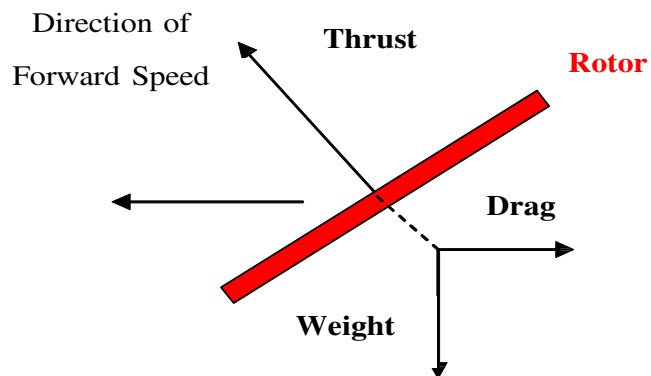
Figure 7.

The produced lift allows the helicopter to rise vertically or hover,



Figure 8.

Tilting the spinning rotor will cause flight in the direction of the tilt



III. CONFIGURATION BASED ON TORQUE REACTION

If you spin a rotor using an engine, the rotor will rotate, but the engine and the helicopter will try to rotate in the opposite direction (TORQUE REACTION)



Figure 9.

Several methods are developed to counter the reaction torque to hold the helicopter straight

1. Tail-Rotor Configuration

One of the classical solution is using a small rotor at the end of a long boom (Tail-Rotor Configuration) to push the fuselage in the opposite direction of the torque force.

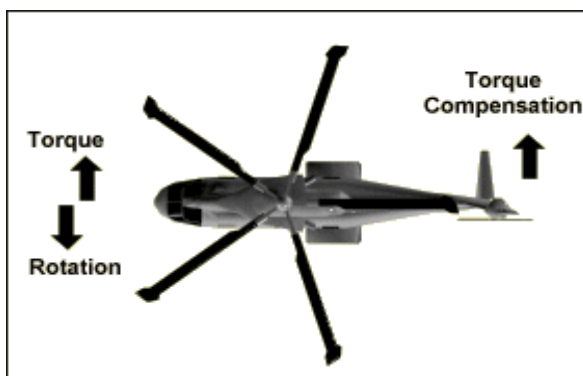


Figure10. Tail-Rotor Configuration

Tandem

Because of the opposite rotation of the rotors, the torque of each single rotor will be neutralized.

It is able to lift heavy loads whose position relative to the helicopter's center of gravity is less critical than the single rotor configuration, Used with big helicopters. The construction of the control system is much more complicated, compared to a helicopter.



Figure 10.

Side by Side

Allow a wide variation of CG position. This design was used for the biggest helicopter built but it was never very successful. Extra drag is created caused by the supporting pylons.

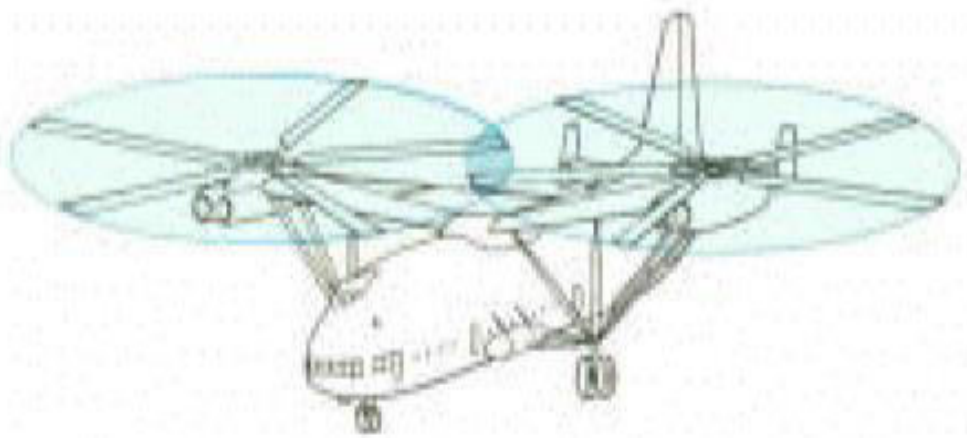


Figure 11.

Coaxial Rotor

This configuration is compact which explains why it is often seen on board ships. The control along the vertical axis occurs as a result of different lifts of the two rotor discs. Depending on which rotor produces more lift, the helicopter will turn to the left or right. For these helicopters it is not possible to reach a high cruising speed, because the drag is too large.

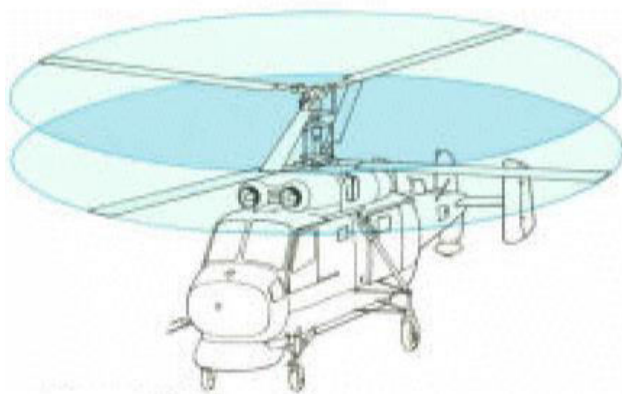


Figure 12.

No-Tail-Rotor (NOTAR) Helicopter

Jet thrust is used rather than blades to Provide directional stability Reduce noise, providing the world's quietest helicopter Counter the main rotor torque.

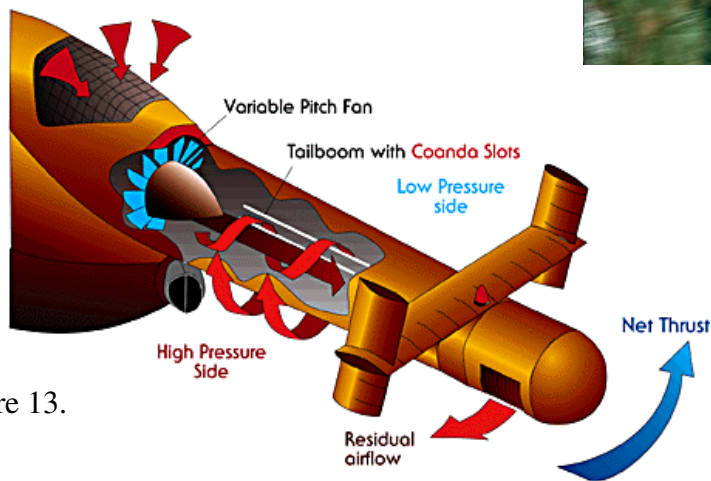


Figure 13.



SATHYABAMA

INSTITUTE OF SCIENCE AND TECHNOLOGY

(DEEMED TO BE UNIVERSITY)

Accredited "A" Grade by NAAC | 12B Status by UGC | Approved by AICTE

www.sathyabama.ac.in

**SCHOOL OF MECHANICAL ENGINEERING
DEPARTMENT OF AERONAUTICAL ENGINEERING**

UNIT – II – IDEAL ROTOR THEORY – SAE1608

I. INTRODUCTION TO HOVERING

Hovering is a maneuver in which the helicopter is maintained in nearly motionless flight over a reference point at a constant altitude and on a constant heading.

To maintain a hover over a point, use sideview and peripheral vision to look for small changes in the helicopter's attitude and altitude. When these changes are noted, make the necessary control inputs before the helicopter starts to move from the point.

To detect small variations in altitude or position, the main area of visual attention needs to be some distance from the aircraft, using various points on the helicopter or the tip-path plane as a reference.

The lifting rotor is assumed to be in hovering condition when both the rotor and the air outside the slip stream are stationary, that is, there is no relative velocity between the rotor and the air outside the slip stream. The airflow developed due to the rotor is confined inside a well-defined imaginary slip stream, as shown in Figure 2.1. There is an axial symmetry in the airflow inside the slip stream.

The hovering theory (or momentum theory) was formulated for marine propellers by W. J. Rankine in 1865 and was later developed by R. E. Froude in 1885. Subsequently, Betz (1920) extended the theory to include rotational effect.

II. MOMENTUM THEORY

Momentum theory is based on the basic conservation laws of fluid mechanics (i.e., conservation of mass, momentum, and energy). The rotor is continuously pushing the air down. As a result, the air in the rotor wake (inside the slip stream) acquires a velocity increment or a momentum change. Hence, as per Newton's third law, an equal and opposite reaction force, denoted as rotor thrust, is acting on the rotor due to air. It may be noted that the velocity increment of the air is directed opposite to the thrust direction.

Assumptions of Momentum Theory

The rotor is assumed to consist of an infinite number of blades and may therefore be considered as an "actuator disk." The actuator disk is infinitely thin so that there is no discontinuity in the velocity of air as it flows through the disk. The rotor is uniformly accelerating the air through the disk with no loss at the tips. The axial kinetic energy imparted to the air in the slip stream is equal to the power required to produce the thrust. In addition, air

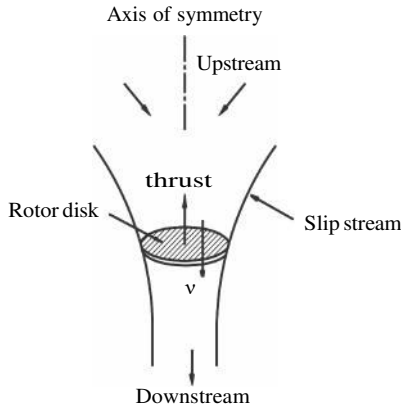


Figure 14. Rotor disk and slip stream .

It is assumed to be incompressible and frictionless. There is no profile drag loss in the rotor disk, and the rotational energy (swirling motion of air) imparted to the fluid is ignored.

NOT E: The actuator disk model is only an approximation to the actual rotor. The momentum theory is not concerned with the details of the rotor blades or the flow, and hence, this theory by itself is not sufficient for designing the rotor system. However, it provides an estimate of the induced power requirements of the rotor and also of the ideal performance limit. The slip stream of the actuator disk in hovering condition is shown in Figure 15.

The rotor disk is represented by a thin disk of area $A (= \pi r^2)$; the far field upstream is denoted as station 1, and the far field downstream is denoted as station 4. The pressure of air at stations 1 and 4 is atmospheric pressure P .

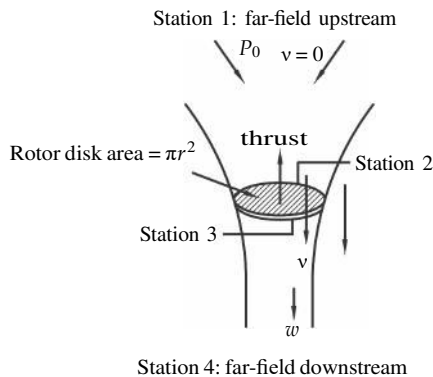


Figure 15. Flow condition in the slip stream.

Stations 2 and 3 represent the locations just above and below the rotor disk, respectively. It is assumed that the loading is uniformly distributed over the disk area. The induced velocity or inflow velocity is v at the rotor disk, and w is the far field wake-induced velocity. The fluid is assumed to be incompressible, having a density ρ . The conservation laws are as follows:

Mass flow rate is given as

$$\dot{m} = \rho A v \quad (2.1)$$

Momentum conservation is obtained by relating the force to the rate of momentum change, which is given as

$$T = \dot{m} (w - 0) = \rho A v w \quad (2.2)$$

Energy conservation relates the rate of work done on the air to its change in kinetic energy per second, which is given as

$$T v = \frac{1}{2} \dot{m} (w^2 - 0) = \frac{1}{2} \dot{m} w^2 \quad (2.3)$$

Substituting for \dot{m} from Equation 2.1 and using Equation 2.2, Equation 2.3 can be written as

$$\rho A v w v = \frac{1}{2} \rho A v \cdot w^2$$

Cancelling the terms results in

$$v = \frac{1}{2} w \Rightarrow w = 2v \quad (2.4)$$

This shows that the far field-induced velocity is twice the induced velocity at the rotor disk.

Substituting for w in Equation 2.2, the expression for rotor thrust in terms of induced velocity at the rotor disk is given by

Rotor thrust:

$$T = \rho A v 2v \quad (2.5)$$

or the induced velocity is given as

$$v = \sqrt{\frac{T}{2\rho A}} \quad (2.6)$$

The induced power loss or the power required to develop the rotor thrust T is given as

$$P = Tv = T \sqrt{\frac{T}{2\rho A}} \quad (2.7)$$

The induced power per unit thrust for a hovering rotor can be written as

$$\frac{P}{T} = v = \sqrt{\frac{T}{2\rho A}} \quad (2.8)$$

The above expression indicates that, for a low inflow velocity, the efficiency is higher. This is possible if the rotor has a low disk loading (T/A). In general, the disk loading of helicopters is of the order of 100–500 N/m², which is the lowest disk loading for any vertical take-off and landing (VTOL) vehicle. Therefore, the helicopters have the best hover performance. Note that the parameter determining the induced power is essentially $T/(\rho A)$. Therefore, the effective disk loading increases with an increase in altitude and temperature.

The pressure variation along the slip stream can be determined from the steady-state Bernoulli equation. The pressure between stations 1 and 2 and between stations 3 and 4 are related, respectively, as

$$p_0 = p_1 + \frac{1}{2} \rho v^2 \quad \text{between stations 1 and 2} \quad (2.9)$$

and

$$p + \frac{1}{2}\rho v^2 = p + \frac{1}{2}\rho w^2 \quad \text{between stations 3 and 4} \quad (2.10)$$

The pressure variation along the slip stream is shown in Figure 16. There is a pressure jump across the rotor disk even though the velocity is continuous.

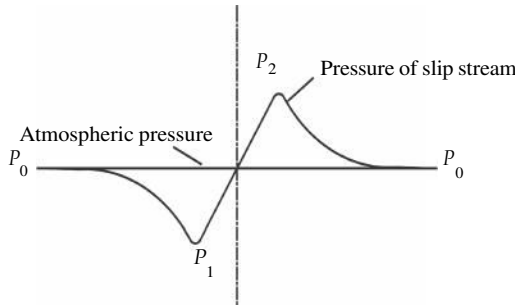


FIGURE 16
Pressure variation along the slip stream.

The jump in pressure is caused by the power given to the rotor to push the air downstream.

From Equations 2.9 and 2.10, the rotor thrust can be evaluated.

$$T = (p_2 - p_1) A = \frac{1}{2}\rho w^2 A = \frac{1}{2}\rho(2v)^2 A = 2\rho Av^2 \quad (2.11)$$

The various quantities can be written in nondimensional form. Using the tip speed ΩR of the rotor blade as reference, the rotor inflow is represented in nondimensional form as

$$\text{Inflow ratio: } \lambda = \frac{v}{\Omega R} = \sqrt{\frac{C_T}{2}} \quad (2.12)$$

Thrust coefficient C_T and power coefficient C_P are defined, respectively, as

$$\text{Thrust coefficient: } C_T = \frac{T}{\rho A(\Omega R)^2} \quad (2.13)$$

$$\text{Power coefficient: } C_P = \frac{P}{\rho A(\Omega R)^3} = \frac{T}{\rho A(\Omega R)^2} \frac{v}{\Omega R} = \frac{C_T^{3/2}}{\sqrt{2}} \quad (2.14)$$

The hovering efficiency of the rotor is defined as

$$M = \frac{\text{minimum power required to hover (ideal power)}}{\text{Actual power required to hover}} = \frac{Tv}{P_{\text{actual}}} \quad (2.15)$$

M is called the figure of merit (FM). The ideal value of M is equal to 1. However, for practical rotors, the value will be less than 1. For good rotors, M is in the range of 0.75 to 0.8. For inefficient rotors, FM will have a value around 0.5. FM can be used for comparing the efficiency of different rotor systems. It should be noted that FM is defined only for the hovering condition of the rotor.

III. BLADE ELEMENT THEORY

Blade element theory (BET) is the foundation for all analyses of helicopter dynamics and aerodynamics because it deals with the details of the rotor system. This theory relates the rotor performance and the dynamic and aeroelastic characteristics of the rotor blade to the detailed design parameters. In contrast, although momentum theory is useful to predict the rotor-induced velocity for a given rotor thrust, it cannot be used to design the rotor system and the rotor blades.

The basic assumption of BET is that the cross section of each rotor blade acts as a two-dimensional airfoil to produce aerodynamic loads, that is, sectional lift, drag, and pitching moment. The effect of the rotor wake is entirely represented by an induced angle of attack at each cross section of the rotor blade. Therefore, this theory requires an estimate of the wake-induced velocity at the rotor disc. This quantity can be obtained either from the simple momentum theory (as given in the previous section) or from more complex theories, such as the prescribed wake or the free wake vortex theories, or nonuniform inflow calculations using acceleration potential.

History of the Development of BET

The origin of BET can be attributed to the work of Willium Froude (1878). However, the first major treatment was by Stefan Drzewiecki, during 1892 to 1920. Drzewiecki considered different blade sections to act independently but was not certain about the aerodynamic characteristics to be used for the air-foils. The two velocity components considered in the theory are (1) tangential velocity Ωr due to rotation and (2) axial velocity V of the propeller. Note that the inflow component at the rotor disk was not included. In Drzewiecki's calculations, the estimated performance exhibited a significant error, which was attributed to the airfoil characteristics. Since the aspect ratio affects the aerodynamic characteristics (in fixed wings), Drzewiecki proposed that the three-dimensional wing characteristics (with appropriate aspect ratio) be used in the BET. The results of this theory had the correct general behavior but were found to be quantitatively inaccurate.

Several attempts (Betz [1915] and Bothezat [1918]) were made to include the increased axial velocity from the momentum theory into the BET. However, Prandtl's finite wing theory provided a proper framework for the correct treatment and inclusion of the influence of the propeller wake on the aerodynamic environment at the blade section. In fixed wing, the lifting line theory is used for the

calculation of induced velocity from the properties of the vortex wake. Thus, following the same approach, the vortex wake was used to define the induced velocities at each cross section of the rotor blade. This theory is called the “vortex theory.” It was through this approach rather than through the momentum theory that induced velocity was finally incorporated correctly in the BET. Therefore, during the initial stages of development, the vortex theory dominated the momentum theory in evaluating the inflow at the rotor disk. The vortex theory is also regarded as a reliable approach in both fixed and rotary wing analyses.

BET for Vertical Flight

In this section, as a general case, BET is applied to a rotor that has a vertical velocity. If the vertical velocity term is set equal to zero, it represents the hovering condition of the rotor. While developing the BET, several assumptions are made. The important assumptions are as follows:

1. In the preliminary highly simplified case, the rotor blade is assumed to be a rigid beam with no deformation. The blade can have a pretwist. (The effects of blade deformation will be considered in later chapters.)
2. The rotor system is rotating with a constant angular velocity Ω .
3. The plane of rotation of the rotor blades is perpendicular to the shaft.
4. The rotor is operating at low disk loading, i.e., a small value of inflow velocity.
5. Compressibility and stall effects are neglected.

Figure 17 shows a rotor system along with the nonrotating hub fixed

axes system ($X_H - Y - Z_I$) and the rotating blade fixed axes system ($X_I - Y_I - Z_I$). Figure 18 shows a typical cross section of the rotor blade at a radial distance r from the center of rotation (or the hub center), various velocity components, and the resultant forces acting on the airfoil section. The blade is set at a pitch angle θ measured from the plane of rotation. U_T and U_P are, respectively, tangential and the perpendicular relative air velocity components, as viewed by an observer on the blade section.

In vertical flight condition, U_P consists of the climb velocity V_C of the helicopter (or rotor) and the induced velocity v . Note that $V_C = 0$ for hovering Condition. The tangential component of velocity U_T is due to rotor rotation. Z, Z

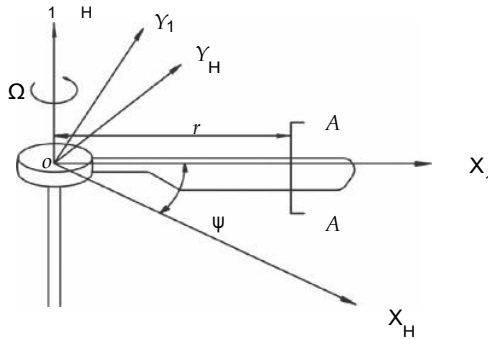


FIGURE 17
Nonrotating hub fixed and rotating blade fixed coordinate systems.

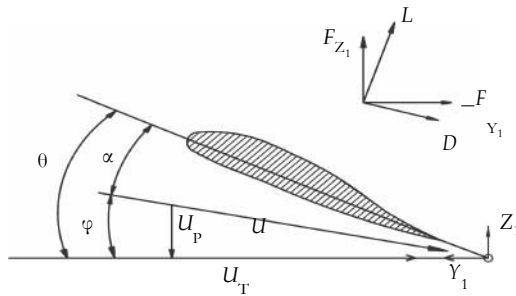


FIGURE 18
Typical cross section of a rotor blade at radial location r and the velocity components.

The relative air velocity components U_T and U_P for vertical flight can be written as

$$U_T = \Omega r \quad \text{and} \quad U_P = V_C + v \tag{2.16}$$

The resultant air velocity U and the inflow angle are given by

$$U = \sqrt{U_T^2 + U_P^2}$$

$$\tan \phi = \frac{U_P}{U_T} \tag{2.17}$$

It can be seen that the vertical component of velocity U_P modifies the angle of attack. Thus, the effective angle of attack at the blade section is given as

$$\alpha = \theta - \phi \tag{2.18}$$

The sectional lift and drag forces can be written as

$$L = \frac{1}{2} \rho U^2 C C_l$$

$$D = \frac{1}{2} \rho U^2 C C_d \tag{2.19}$$

where C is the blade chord, and C_l and C_d are, respectively, the lift and drag aerodynamic coefficients, which are functions of the angle of attack and the Mach number. Resolving these two sectional forces along parallel and perpendicular directions to the rotor disk, the vertical and horizontal (or in- plane) force components can be obtained as

$$\begin{aligned} F_z &= L \cos \phi - D \sin \phi \\ -F_{y1} &= L \sin \phi + D \cos \phi \end{aligned} \quad (2.20)$$

Combining the forces due to all the blades in the rotor system, the elemental thrust, torque, and power due to all the blades in the rotor system can be obtained. The following expressions are obtained by noting that the sectional forces acting on the blade cross section at a radial distance r are the same on all the blades.

$$\begin{aligned} dT &= N F_z dr \\ dQ &= -N F_{y1} r dr \\ dP &= \Omega |dQ| = N |F_{y1}| \Omega r dr \end{aligned} \quad (2.21)$$

Where N is the total number of blades in the rotor system. The negative sign in the torque expression indicates that aerodynamic drag force on the blade provides a clockwise torque when the rotor is rotating in a counterclockwise direction, as shown in Figure 2.1. The positive quantity of the torque essentially represents the torque applied to the rotor by the engine to keep the rotor rotating at the prescribed angular velocity.

Assuming that $U_P \ll U$, one can make a small angle assumption for the inflow angle. Note that this assumption is not valid near the blade root. However, since the dynamic pressure near the root is very small, the aerodynamic loads are also of small magnitude. Hence, the error due to the small angle assumption can be considered to be negligible. In addition, due to root cutout, the cross sections near

the root (~20% of the rotor radius) do not produce any significant aerodynamic lift.

Making a small angle assumption, one can write

$$\begin{aligned} \cos\phi &\approx 1 \\ \sin\phi &\approx \phi \approx \frac{U_P}{U_T} \end{aligned} \tag{2.22}$$

$$U \approx U_T$$

$$\text{and } C_l = a\alpha = a(\theta - \phi)$$

where a is the lift curve slope.

Substituting the above approximations, the expressions for lift and drag per unit length, from Equation 2.19, can be written as

$$\begin{aligned} L &\equiv \frac{1}{2}\rho U_T^2 C_n \left(\theta - \frac{U_P}{U_T} \right) = \frac{1}{2}\rho C_n (U_T^2 \theta - U_P U_T) \\ D &\approx \frac{1}{2}\rho U_T^2 C_d \end{aligned} \tag{2.23}$$

Also, the force components can be approximated as

$$\begin{aligned} F_z &\approx L \\ -F_{y1} &\approx L\phi + D \end{aligned} \tag{2.24}$$

Using this approximation, the elemental thrust, torque (applied torque), and power (Equation 2.21), can be expressed as

$$\begin{aligned} dT &\approx N L dr \\ dQ &\approx N (L\phi + D) r dr \\ dP &\approx N (L\phi + D) \Omega r dr \end{aligned} \tag{2.25}$$

The elemental thrust, torque, and power quantities can be nondimension- alized by using appropriate reference quantities, as

$$\begin{aligned}
 dC_T &= \frac{dT}{\rho A (\Omega R)^2} \\
 dC_Q &= \frac{dQ}{\rho A (\Omega R)^2 R} \\
 dC_P &= \frac{dP}{\rho A (\Omega R)^3}
 \end{aligned}
 \tag{2.26}$$

Thrust Coefficient

Using Equations 2.16, and 2.23 to 2.26, the elemental thrust coefficient can be written as

$$\begin{aligned}
 dC_T &= \frac{N \frac{1}{2} \rho (\Omega r) C_n [\Omega r \theta - (V_c + v)] dr}{\rho \pi R^2 (\Omega R)^2} \\
 dC_T &= \frac{1}{2} \frac{NC}{\pi R} a [\theta \bar{r}^2 - \lambda \bar{r}] d\bar{r} \\
 dC_T &= \frac{\sigma a}{2} [\theta \bar{r}^2 - \lambda \bar{r}] d\bar{r}
 \end{aligned}
 \tag{2.27}$$

Solidity ratio is defined as $\sigma = \text{blade area}/\text{rotor disk area}$, where $\sigma = \frac{NCR}{\pi R^2}$ is the solidity ratio for the constant chord blade.

$\lambda = \frac{V_c + v}{\Omega R}$ is the total inflow ratio

$$\bar{r} = \frac{r}{R} \quad (2.28)$$

The differential expressions can be integrated over the length of the blade by assuming a constant chord, and a uniform inflow.

The thrust coefficient is obtained as

$$C_T = \int_0^1 \frac{\sigma a}{2} [\theta \bar{r}^2 - \lambda \bar{r}] d\bar{r} \quad (2.29)$$

Assuming a linear twist variation for the blade pitch angle along the span of the blade as

$$\theta = \theta_0 + \bar{r}\theta_{tw} \text{ (or } \theta = \theta_{0.75} + (\bar{r} - 0.75)\theta_{tw}) \quad (2.30)$$

where θ_{tw} , θ_0 , and $\theta_{0.75}$ are the blade twist rate due to the pretwist of the blade, the pitch angles at the blade root, and at a radius $0.75 R$, respectively. Substituting Equation 2.30 in Equation 2.29 and integrating over the length of the blade, the thrust coefficient becomes

$$C_T = \frac{\sigma a}{2} \left[\frac{\theta_{0.75}}{3} - \frac{\lambda}{2} \right] \quad (2.31)$$

On the other hand, a twist distribution of $\theta = \frac{\theta_{tp}}{\bar{r}}$ (known as the "ideal twist distribution") results in a thrust coefficient expression given as

$$C_T = \frac{\sigma a}{4} [\theta_{tp} - \lambda] \quad (2.32)$$

This ideal twist distribution, while physically not possible to achieve, is of interest because it gives a uniform inflow over the rotor disk for constant chord blades. This twist distribution is denoted as ideal twist distribution

because the momentum theory shows that uniform inflow provides a minimum induced power loss.

Now, it is shown that BET provides a relationship between rotor thrust coefficient, pitch angle, and inflow ratio. On the other hand, momentum theory gives a relationship between thrust coefficient and inflow ratio.

For hovering condition, in the case of constant chord and a linearly twisted blade, thrust coefficient is written as (note: $V_c = 0$)

$$C_T = \frac{\sigma a}{2} \left[\frac{\theta_{0.75}}{3} - \frac{\lambda}{2} \right] \quad (2.33)$$

From the momentum theory, the inflow ratio in hover is given as (Equation 2.12)

$$\lambda = \sqrt{\frac{C_T}{2}}$$

Combining the above two expressions, the relationship between $\theta_{0.75}$ and C_T can be written as

$$\theta_{0.75} = \frac{6C_T}{\sigma a} + \frac{3}{2} \sqrt{\frac{C_T}{2}} \quad (2.34)$$

The first term corresponds to the mean angle of attack of the rotor blade, while the second term is the additional pitch angle required due to the induced inflow. The above three relationships can be used to obtain an estimate of the thrust coefficient, the pitch angle at 0.75 R , and the inflow ratio under hovering condition.

Using Equations 2.12 and 2.33, a relationship between the inflow ratio and the blade pitch angle $\theta_{0.75}$ can be obtained as

$$\lambda = \frac{\sigma a}{16} \left\{ \sqrt{1 + \frac{64}{3\sigma a} \theta_{0.75}} - 1 \right\} \quad (2.35)$$

Torque/Power Coefficient

The elemental torque and power coefficients can be obtained from Equations 2.16, 2.23, 2.25, and 2.26. They are shown to be equal, and it is given as

$$dC_p = dC_Q = \left[\frac{\sigma u}{2} (\bar{U}_r \bar{U}_r \theta - \bar{U}_r^2) + \frac{\sigma C_d}{2} \bar{U}_r^2 \right] \bar{r} d\bar{r} \quad (2.36)$$

$$dC_p = dC_Q = \left[\frac{\sigma u}{2} (\theta \bar{r} \lambda - \lambda^2) + \frac{\sigma C_d}{2} \bar{r}^2 \right] \bar{r} d\bar{r}$$

The velocity quantities with overbar represent nondimensional quantities obtained by dividing with reference velocity ΩR , which is the tip speed of the rotor blade.

The elemental power coefficient can be written as

$$dC_p = \left[\lambda \frac{\sigma u}{2} (\theta \bar{r}^2 - \lambda \bar{r}) + \frac{\sigma C_d}{2} \bar{r}^3 \right] d\bar{r} \quad (2.37)$$

Noting from Equation 2.27 that the first term contains an elemental thrust coefficient, Equation 2.37 can be written as

$$dC_p = \lambda dC_T + \frac{\sigma C_d}{2} \bar{r}^3 d\bar{r} \quad (2.38)$$

Integrating both sides over the rotor system, the power coefficient can be obtained as

$$C_p = \int \lambda dC_T + \int \frac{\sigma C_d}{2} \bar{r}^3 d\bar{r} \quad (2.39)$$

$$C_p = C_{pi} + C_{pnd}$$

The power coefficient C_{pi} represents the power loss due to total induced flow, and C_{pnd} is the power loss due to profile drag.

For uniform inflow, the power due to total induced flow is $C_{pi} = \lambda C_T$.

Since total inflow $\lambda = \frac{V_c + v}{\Omega R}$, during climb, C_{pi} includes the power required for climbing as well as the induced power loss. Therefore, one can write the induced power in terms of two quantities, namely climb power and induced power, that is,

$$C_{pi} = C_{pc} + C_{pv}$$

In other words, this power term can be expressed as

$$P_i = P_c + P_v = V_c T + vT = (V_c + v)T \quad (2.40)$$

During hover $\lambda = \sqrt{\frac{C_T}{2}}$, therefore, the induced power loss becomes

$$C_{P_i} = C_{P_{i_e}} = \frac{C_T^{3/2}}{\sqrt{2}} \quad (2.41)$$

This is the induced power loss in hover under ideal condition. However, for a real rotor with a practical twist, a planform, and a finite number of blades, the induced power loss will be higher than the ideal value $\frac{C_T^{3/2}}{\sqrt{2}}$. One way to compute the induced power loss is to integrate $\int \lambda dC_T$ under real conditions, taking into account the nonuniform inflow over the rotor disk. On the other hand, one can use the same expression as the momentum theory expression for power loss but with an empirical factor κ to account for the additional losses due to the real situation, that is,

$$C_{P_i} = \frac{\kappa C_T^{3/2}}{\sqrt{2}} \quad (2.42)$$

The factor κ accounts for nonideal conditions, and its value is usually taken as 1.15, which implies an additional power of about 15% more than the ideal power.

Next, consider the profile power term from Equation 2.39, which is given as

$$C_{P_{pd}} = \int \frac{\sigma C_d}{2} \bar{r}^3 d\bar{r} \quad (2.43)$$

Assuming the constant chord for the blade with the drag coefficient $C_d = C_{d_0}$ (a constant), the profile power loss can be obtained by integrating over the rotor radius. It is given as

$$C_{P_{pd}} = \frac{\sigma C_{d_0}}{8} \quad (2.44)$$

Combining Equations 2.42 and 2.44, the total power loss in hover can be expressed as

$$C_P = \kappa \frac{C_T^{3/2}}{\sqrt{2}} + \frac{\sigma C_{d_0}}{8}$$

The efficiency of the rotor is expressed as the ratio of the ideal power over the actual power. This ratio is denoted as figure of merit, which is given by

$$M = \frac{C_P \text{ ideal}}{C_{P1} + C_{Ppd}} = \frac{\frac{C_T^{3/2}}{\sqrt{2}}}{\kappa \frac{C_T^{3/2}}{\sqrt{2}} + \frac{\sigma C_{d0}}{8}} \quad (2.45)$$

A plot of figure of merit M as a function of thrust C_T (for a set of given values of (σ, C_{d0}, κ)) is shown in Figure 2.6. It can be noted from the figure that, for low values of thrust coefficient, due to a comparatively high value of profile drag, the figure of merit is low. Thus, the rotor is not operating efficiently. As C_T increases, the figure of merit increases. For high values of C_T ($\approx 0.006-0.01$), figure of merit does not show a large variation. This functional form indicates that figure of merit asymptotically approaches unity as the C_T is increased. In practical situations, for a large value of C_T , the angle of attack has to be large, which can lead to blade stall and an associated increase in drag. Hence, there will be a reduction in figure of merit.

Figure of merit is a useful parameter for comparing the efficiency of different rotors having the same disk loading. For a given value of C_T , figure of merit M will have a high value for a low value of solidity ratio σ and drag coefficient C_{d0} . If the rotor solidity is too low, a high value of angle of attack will be required to achieve the given thrust (Equation 2.34). Therefore, the rotor should have as low a value of solidity as possible with an adequate stall margin for the airfoil. Blade twist and variable chord also influence the induced and profile power losses. A study of these effects requires a more detailed analysis, which can be taken as an exercise.

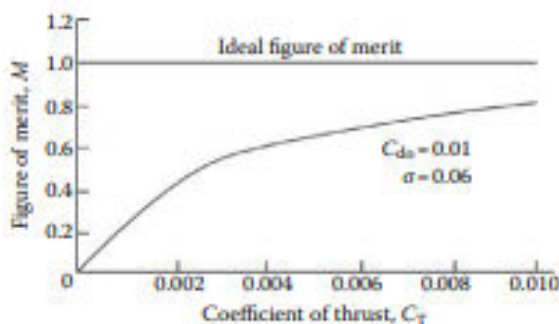


Figure 19. Variation of figure of merit with thrust coefficient.

IV. MOMENTUM THEORY FOR VERTICAL FLIGHT

Vertical flight of the helicopter at a speed V includes climb ($V > 0$), hover ($V = 0$), descent ($V < 0$), and also the special case of autorotation (i.e., power-off descent). Between hover and autorotation descend speed, the helicopter is descending at a reduced power. At autorotation descend speed, the helicopter rotor does not require any power to keep the rotor rotating. Beyond autorotation descend speed, the rotor is actually generating power. An interpretation of induced power losses requires a discussion of the flow states of the rotor in axial flight. Consider two cases of the actuator disk theory, namely vertical climb and vertical descent. Assume that the flow is uniform in the slip stream. Figure 20 shows the velocity profile in both cases. The arrows represent the positive direction of flow velocity in the slip stream. It may be noted that, for climb, velocity V is positive, and for descent, it is negative. In the following, the derivation of the induced velocity expression for both climb and descent is provided side by side.

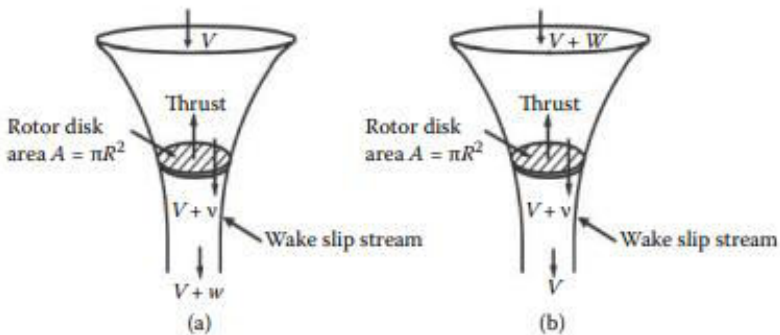


Figure 20. Flow velocity in climb and decent. (a) climb ($V > 0$). (b) Decent ($V < 0$)

Since the induced velocity in hover is given as $v_h^2 = \frac{T}{2\rho A}$, and assuming that the actuator disk in steady vertical flight is supporting the same weight as in hover (i.e., $T = T_h = \rho A 2v^2$). Equating the thrust expressions in hover and vertical flight, the equation for the induced flow v can be obtained for both climb and descent as

Climb ($V > 0$)	Descent ($V < 0$)
Mass flow through the rotor disk	
$\dot{m} = \rho A(V + v)$	$\dot{m} = \rho A(V + v)$
Momentum conservation	
$T = \dot{m}(V + w) - \dot{m}V = \dot{m}w$	$T = \dot{m}V - \dot{m}(V + w) = -\dot{m}w$
Energy conservation	
$P = \frac{1}{2} \dot{m}(V + w)^2 - \frac{1}{2} \dot{m}V^2$	$P = \frac{1}{2} \dot{m}V^2 - \frac{1}{2} \dot{m}(V + w)^2$
Simplifying,	
$P = \frac{1}{2} \dot{m}(2Vw + w^2)$	$P = -\frac{1}{2} \dot{m}(2Vw + w^2)$
Since $P = T(V + v)$, we have	
$\dot{m}w(V + v) = \frac{1}{2} \dot{m}(2Vw + w^2)$	$-\dot{m}w(V + v) = -\frac{1}{2} \dot{m}(2Vw + w^2)$
$w = 2v$	$w = 2v$
Hence, thrust	
$T = \rho A(V + v)2v$	$T = -\rho A(V + v)2v$

Climb ($V > 0$)

$$\frac{v}{v_h} \left(\frac{V}{v_h} + \frac{v}{v_h} \right) = 1$$

Descent ($V < 0$)

$$\frac{v}{v_h} \left(\frac{V}{v_h} + \frac{v}{v_h} \right) = -1$$

Solving these equations, the induced velocity $\frac{v}{v_h}$ as a function of V can be obtained for climb and descent flight conditions,

Note that induced velocity $\frac{v}{v_h}$ is always positive. Hence, it may be noted that the negative root of the radical is not valid for climb, but for descent, both the positive and negative roots of the radical will provide a positive induced velocity. It will be shown later that the positive root of the radical is not a valid root due to the physical condition of the flow.

Climb ($V > 0$)

$$\frac{v}{v_h} = -\frac{V}{2v_h} + \sqrt{\left(\frac{V}{2v_h}\right)^2 + 1} \quad (2.59a)$$

Descent ($V < 0$)

$$\frac{v}{v_h} = -\frac{V}{2v_h} \pm \sqrt{\left(\frac{V}{2v_h}\right)^2 - 1} \quad (2.59b)$$

The net flow velocity at the rotor disk is

Climb ($V > 0$)

$$\frac{V+v}{v_h} = \frac{V}{2v_h} + \sqrt{\left(\frac{V}{2v_h}\right)^2 + 1} \quad (2.60a)$$

Descent ($V < 0$)

$$\frac{V+v}{v_h} = \frac{V}{2v_h} \pm \sqrt{\left(\frac{V}{2v_h}\right)^2 - 1} \quad (2.60b)$$

The net velocity at the far wake is

Climb ($V > 0$)

$$\frac{V+2v}{v_h} = +\sqrt{\left(\frac{V}{v_h}\right)^2 + 4}$$

Descent ($V < 0$)

$$\frac{V+2v}{v_h} = \pm\sqrt{\left(\frac{V}{v_h}\right)^2 - 4}$$

Using Equations 2.59a and 2.59b, the variation of induced velocity $\frac{v}{v_h}$ versus climb (or descent) velocity $\frac{V}{v_h}$ is plotted, and it is shown in Figure 21. The dashed portions of the curve are branches of the solution, which are extrapolated beyond the assumed conditions.

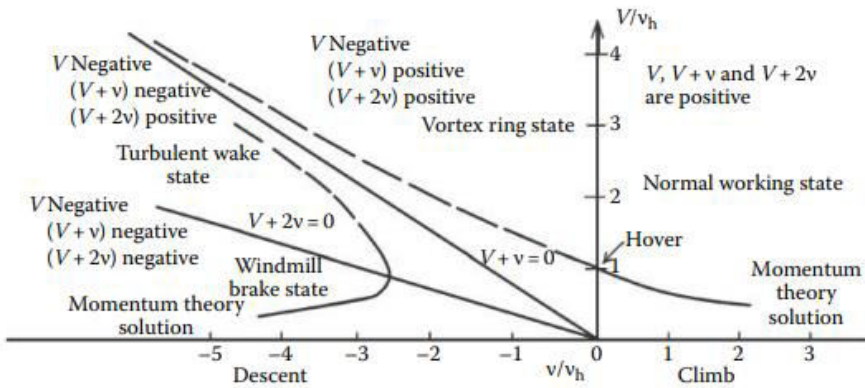


Figure 21. Variation of induced flow as a function of climb and descent speed

These dashed lines do not correspond to the assumed flow state. The line $V + v = 0$ is where the direction of flow through the rotor disk and the total induced power $P = T(V + v)$ change sign. At the line, $V + 2v = 0$, the flow in the far wake changes sign. The three lines $V = 0$, $V + v = 0$, and $V + 2v = 0$ divide the graph into four regions. These regions are denoted as the normal working state (hover and climb), the vortex ring state, the turbulent wake state, and the windmill brake state. The flow characteristics in each of the states are described below.

Normal Working State

The normal working state includes climb and hover. During climb, the velocity in the slip stream throughout the flow field is downward, with both V and v positive. For mass conservation,

the wake contracts downstream of the rotor. The momentum theory gives a good estimate of the performance. Hover ($V = 0$) is the limit of the normal working state. Even in hover, the momentum theory gives a good estimate of the performance. The flow pattern in the normal working state is shown in Figure 22.

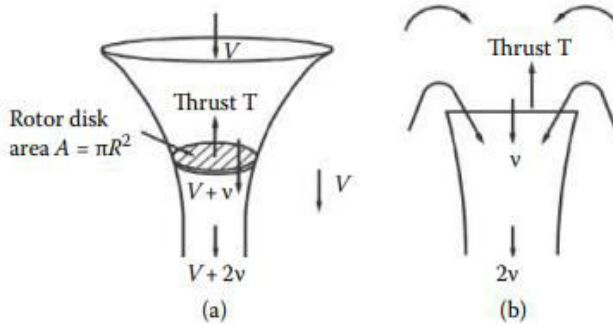


Figure 22. Flow pattern in the normal working state. (a) Climb ($V > 0$). (b) Hover ($V = 0$)

Vortex Ring State

When the rotor starts to descend, definite slip stream ceases to exist because the flow inside the slip stream changes its direction as we move from far upstream to far wake downstream. Therefore, there will be a large recirculation and turbulence. In the vortex ring state, the induced power ($P = T(V + v) > 0$) is positive in the sense that the engine has to supply power to the rotor to keep it rotating. The flow pattern and the directions of the flow are shown in Figure 23.

The flow pattern in the vortex ring state is like that of a vortex ring in the plane of the rotor disk. The upward velocity in the free stream keeps the tip vortices piled up as a ring. As the strength builds up, it breaks away from the disk plane, leading to a sudden breakdown of the flow. The flow is highly unsteady and produces a highly disturbing low-frequency vibration.

The momentum theory is not valid since the flows inside the slip stream are in opposite directions. The limiting case of the vortex ring state is when the flow through the disk is zero, that is, $V + v = 0$. It may be noted that, during descent, $V < 0$ and induced velocity $v > 0$. Hence, the power required for the induced flow v

is exactly equal to the gain in power due to descent. This state corresponds to ideal autorotation (in the absence of profile power loss).

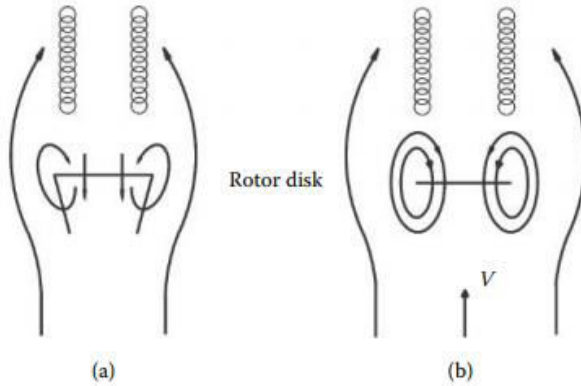


Figure 23. Flow pattern and velocity in the vortex ring state.
 (a) Low descent rates. (b) High descent rates.

Turbulent Wake State

The turbulent wake state corresponds to the region in Figure 21, where $V + v = 0$ to $V + 2v = 0$. Under the condition $V + v = 0$, there is no flow through the rotor disk. In reality, there is a considerable recirculation and turbulence. The flow pattern in the turbulent wake state is shown in Figure 2.14. The flow state is somewhat similar to the flow past a circular plate of the same area of the rotor disk, with no flow through the disk and a turbulent wake behind it.

When the descent speed increases, $V + v < 0$, that is, the flow at the rotor disk is upward with less recirculation through the rotor. The flow above the rotor is highly turbulent. The rotor in this state experiences some roughness due to turbulence, but not like the high vibration in the vortex ring state.

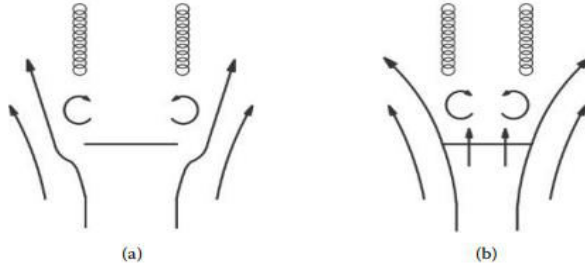


Figure 24. Flow pattern in the turbulent wake state. (a) Ideal autorotation ($V+v=0$). (b) Turbulent wake state

Windmill Brake State

At the high rate of descent ($V < -2v$), the flow once again becomes smooth, with a definite slip stream. The flow is upward throughout the slip stream, and the momentum theory is valid in this condition. In this state, the power $P = T(V + v)$ is less than 0, implying that the rotor is producing power (or power is extracted from the flow).

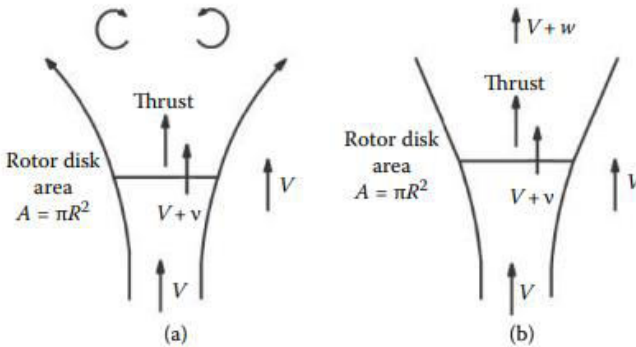


Figure 25. Flow pattern in the windmill brake state. (a) Boundary ($V+2v = 0$). (b) Windmill brake state.

The flow pattern in the windmill brake state is shown in Figure 25. It is important to note that induced velocity is almost impossible to measure in flight. Therefore, the induced velocity curve is drawn by calculating the induced velocity from the power measurements. The power supplied to the rotor can be expressed as a sum of three components, given as

Shaft power = climb power + induced power + profile power

$$P = TV = T v + \frac{\sigma C_{d0}}{8} \rho \pi R^2 (\Omega R)^3 2.61)$$

For given values of shaft power, gross weight ($T = W$), rotor angular velocity, rate of descent, and blade drag coefficient, the mean effective induced velocity can be determined from the above equation.

Another way of presenting the induced velocity variation was developed by Lock (1947). In this representation (Figure 26), the variation of total induced velocity $\left(\frac{V+v}{v_h}\right)$ is plotted as a function of $\frac{V}{v_h}$. This curve is also known as the “universal inflow curve.”

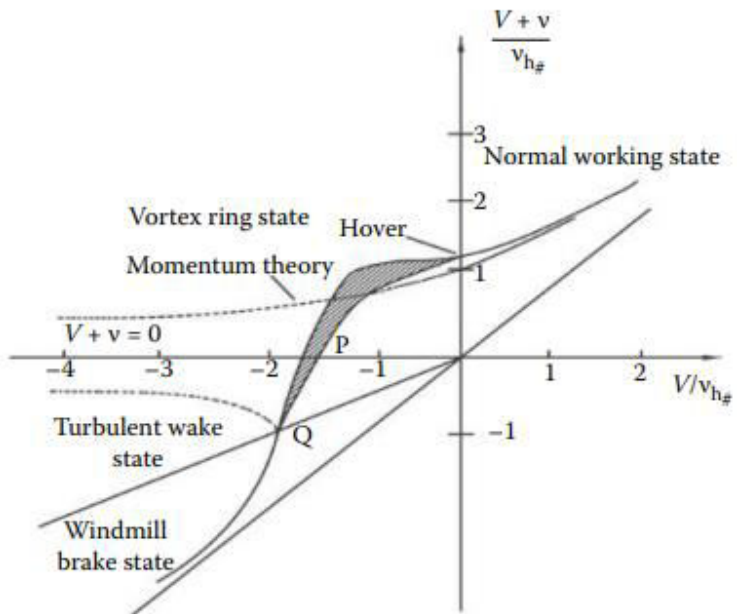


Figure 26. Total inflow as a function of climb and decent speed In the vortex ring and the turbulent wake regions, the inflow curve is represented by a band, corresponding to practical situations. The universal inflow curve crosses the ideal autorotation line at about $\left(\frac{V}{v_h}\right) = -1.71$ (i.e., in the range of -1.6 to -1.8). In practical situations, because of fuselage drag effects, autorotation occurs at a higher rate of descent, which is in the turbulent wake state. In the turbulent wake region, the inflow

curve can be approximated by a straight line PQ. The coordinates of P and Q are, respectively, $(\bar{X}, 0)$ and Q is $(-2, -1)$. The equation of line PQ can be written as

$$\frac{V + v}{v_h} = \frac{-\bar{X}}{2 + \bar{X}} + \frac{1}{2 + \bar{X}} \frac{V}{v_h} \quad (2.62)$$

Where \bar{X} is the intercept at the $\frac{V}{v_h}$ axis. When $\bar{X} = -1.71$, the inflow equation in the turbulent wake state becomes

$$\frac{V + v}{v_h} = 5.9 + 3.4 \frac{V}{v_h} \quad (2.63)$$

Autorotation in Vertical Descent

Autorotation is the state of rotor operation where there is no net power requirement from the power plant. The source of power is due to the decrease in gravitational potential energy. The descent velocity supplies the power to the rotor, and the helicopter is capable of power-off autorotation in vertical flight. It may be noted that the lowest descent rate is achieved in forward flight, which will become obvious when we deal with forward flight power requirements in the following chapter.

The net power to the rotor during autorotation is zero. Hence, from Equation 2.61,

$$P = T(V + v) + P_{pd} = 0 \quad (2.64)$$

In Equation 2.64, the first term represents the power required to generate the thrust to support the weight of the helicopter through total inflow at the rotor disk, and the second term represents the profile power required to drag the rotor blades through air. Using nondimensional parameters, Equation 2.64 can be written as

$$C_T \rho \pi R^2 (\Omega R)^2 \left(\frac{V+v}{v_h} \right) v_h + C_{Ppd} \rho \pi R^2 (\Omega R)^3 = 0 \quad (2.65)$$

or

$$C_T \rho \pi R^2 (\Omega R)^2 \left(\frac{V+v}{v_h} \right) \sqrt{\frac{C_T \rho \pi R^2 (\Omega R)^2}{2 \rho \pi R^2}} + C_{Ppd} \rho \pi R^2 (\Omega R)^3 = 0 \quad (2.66)$$

Using Equations 2.56 and 2.61, Equation 2.66 can be simplified as

$$\frac{V+v}{v_h} = - \frac{C_{Ppd}}{C_T^{3/2} / \sqrt{2}} \propto \frac{C_{d0}}{\sigma^{3/2} C_1^{3/2}} \quad (2.67)$$

This expression indicates that a low value of $\frac{C_{d0}}{C_1^2}$ provides a low

descent velocity in autorotation in vertical descent. Knowing the thrust and profile drag coefficients, the descent rate can be obtained from the universal inflow curve (Figure 2.16). The value of $\frac{V+v}{v_h}$ is typically about -0.3, which is in the turbulent wake state. Since the slope of the curve (the slope is 3.5 from Equation 2.63) is very large in this region, the increase in the descent rate required to overcome profile drag is very small. Tail rotor and other aerodynamic interference losses must also be included in evaluating the autorotation descent rate. Such losses are usually about 15% to 20% of the profile power. The limits of the descent rate in vertical autorotation are essentially the limits of the turbulent wake state (i.e., $\frac{V}{v_h}$ in the range of -1.71 to -2). For practical purposes, one can assume that autorotation occurs for $\frac{V}{v_h} = -1.81$. For typical values of inflow v_h , the autorotation descent velocity is in the range $V = 15$ to 25 m/s. (For the values of helicopter disk loading $T/A = 100$ - 500 N/m², v_h is in the range of 6.4-14 m/s, with density $\rho = 1.225$ kg/m³.) The autorotation performance may also be evaluated in terms of rotor drag coefficient. During steady autorotation descent, the

drag coefficient of the rotor can be defined as

$$C_D = \frac{T}{1/2\rho V^2 A} = \frac{T/(2\rho A)}{V^2/4} = \left(\frac{2}{V/v_h} \right)^2 \quad (2.68)$$

For typical values of $\frac{V}{v_h} = -1.71$ to -1.81 , the drag coefficient has a value in the range of 1.22 to 1.38. For real helicopters, C_D is in the range of 1.1 to 1.3. For comparison, a circular plate of area A has a drag coefficient of about $C_D = 1.28$ and a parachute of frontal area A has $C_D = 1.40$. This shows that a helicopter rotor in power-off descent is quite efficient in producing the thrust to support the helicopter. The rotor is almost as good as a parachute of the same diameter.

V. BLADE ELEMENT THEORY IN VERTICAL FLIGHT

Consider an element of blade of chord c with width dr at a radius r from the axis of rotation. The geometric pitch angle of the blade element relative to the plane of rotation is θ , the climbing speed is V_c , and the local induced velocity is v_i . The direction of the flow relative to the blade makes an angle ϕ (usually called the inflow angle) with the plane of rotation, Fig. 27, and ϕ is given by

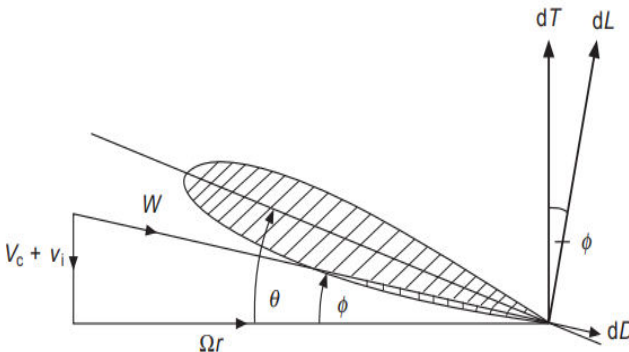


Figure 27 Force components on blade

$$\tan \phi = (V_c + v_i) / \Omega r$$

or, for small φ ,

$$\varphi = (V_c + v_i) / \Omega r$$

The lift on the blade elements is

$$dL = \frac{1}{2} \rho W^2 C_L c dr$$

$$dL = \frac{1}{2} \rho \Omega^2 r^2 C_L c dr$$

Since, for small φ , $W^2 \approx \Omega^2 r^2$

Let us suppose that the lift slope a of the section is constant so that, if the section incidence α is measured from the no-lift line, we can write

$$C_L = a\alpha = a(\theta - \varphi)$$

Empirical data suggests a lift slope of about 5.7. The elementary lift is now

$$dL = \frac{1}{2} \rho \Omega^2 r^2 a(\theta - \varphi) c dr$$

Since φ is usually a small angle, we can write $dL \approx dT$, where dT is the elementary thrust, the force perpendicular to the plane of rotation. The total thrust is therefore

$$dT = \frac{1}{2} \rho \Omega^2 r^2 a(\theta - \varphi) c dr$$

$$T = \frac{1}{2} \rho a b \Omega^2 \int_0^R c(\theta - \varphi) r^2 dr \text{ --- (2.25)}$$

Where b is number of blade

Defining

$$\lambda_c = \frac{V_c}{\Omega R}, \lambda_i = \frac{v_i}{\Omega R} \quad x = \frac{r}{R}$$

eqn 2.25 can be written

$$T = \frac{1}{2} \rho a b \Omega^2 R^3 \int_0^1 c(\theta x^2 - (\lambda_c + \lambda_i)x) dx \text{ --- (2.26)}$$

If the chord, induced velocity, and 'collective' pitch angle θ are constant along the blade, eqn 2.26 can be integrated easily to give

$$T = \frac{1}{2} \rho a c b \Omega^2 R^3 \left(\frac{1}{3} \theta_0 - \frac{1}{2} (\lambda_c + \lambda_i) \right) \text{ --- (2.27)}$$

where θ_0 is the constant (collective) pitch angle.

Defining a thrust coefficient by

$$t_c = \frac{T}{\rho s A \Omega^2 R^2}$$

where $s = bc/\pi R$ is the rotor solidity, eqn 2.27 gives

$$t_c = (a/4)[2\theta_0/3 - (\lambda_c + \lambda_i)] \text{ -----(2.28)}$$

In American work, the thrust coefficient is usually defined by

$$C_T = T/\rho A \Omega^2 R^2$$

So that the two thrust coefficients are related by $t_c = C_T / s$.

From the momentum theory, the induced velocity and the thrust are related by

$$T = 2\rho A (V_c + v_i)v_i \text{ -----(2.11)}$$

which can be written in non-dimensional form as

where $s = bc/\pi R$ is the rotor solidity, eqn 2.27 gives

$$t_c = (a/4)[2\theta_0/3 - (\lambda_c + \lambda_i)] \text{ -----(2.28)}$$

In American work, the thrust coefficient is usually defined by

$$C_T = T/\rho A \Omega^2 R^2$$

So that the two thrust coefficients are related by $t_c = C_T / s$.

From the momentum theory, the induced velocity and the thrust are related by

$$T = 2\rho A (V_c + v_i)v_i \text{ ---- (2.11)}$$

which can be written in non-dimensional form as

$$\lambda_i^2 + \lambda_c \lambda_i - \frac{1}{2} s t_c = 0 \text{ --- (2.29)}$$

The positive root being the correct one to take. With λ_c being given, eqns 2.28 and 2.29 can be solved for t_c if θ_0 is known, or the required pitch angle θ_0 can be calculated if t_c is given. In hovering flight we have simply

$$t_c = (a/4)(2\theta_0/3 - \lambda_i) \text{ ---- (2.30)}$$

And

$$s t_c = 2 \lambda_i^2 \text{ ---- (2.31)}$$

Equations 2.28 and 2.29 have been obtained on the assumption that the blade pitch and chord were constant along the blade and that the downwash velocity had the constant 'momentum' value given by eqn 2.11.

Modern helicopter blades usually have constant chord and approximately linear twist, and, if we assume that a linear variation of induced velocity is quite a good approximation to that obtaining in practice, eqn 2.26 can again be integrated quite easily.

Let us write the local blade pitch as $\theta_0 - \theta_{1x}$ and the local induced velocity as $v_i = v_{iTx}$, where θ_1 is the blade 'washout'

angle and v_{iT} is the downwash velocity at the blade tip. Then eqn 2.26 integrates to give

$$t_c = \frac{a}{4} \left[\frac{2}{3} \left(\theta_0 - \frac{3}{4} \theta_1 \right) - \lambda_c - \frac{2}{3} \lambda_{iT} \right] \dots \dots \dots (2.32)$$

where $\lambda_{iT} = v_{iT}/\Omega R$.

Now it is generally accepted that eqn 2.11 can be expressed in differential form as

$$dT = 4\pi r \rho v_i (V_c + v_i) dr \dots \dots \dots (2.33)$$

where $2\pi r dr$ is the area of the annulus of width dr over which the thrust dT is distributed.

It can be shown that eqn 2.33 is not strictly valid but it has given successful results in airscrew work and may be regarded as sufficiently accurate for most purposes.

It appears to be true for the linearised problem in which we take $V_c + v_i \approx V_c$ and $dT = 4\pi r \rho v_i V_c dr$.

Now it is generally accepted that eqn 2.11 can be expressed in differential form as

$$dT = 4\pi r \rho v_i (V_c + v_i) dr \dots \dots \dots (2.33)$$

where $2\pi r dr$ is the area of the annulus of width dr over which the thrust dT is distributed.

It can be shown that eqn 2.33 is not strictly valid but it has given successful results in airscrew work and may be regarded as sufficiently accurate for most purposes.

It appears to be true for the linearised problem in which we take $V_c + v_i \approx V_c$ and $dT = 4\pi r \rho v_i V_c dr$.

Then putting $v_1 = v_{iT} \times$ in eqn 2.33 and integrating gives

$$T = \rho \pi R^2 (v_{iT}^2 + 4v_{iT}V_c/3)$$

or, in coefficient form,

$$\lambda_{iT}^2 + 4\lambda_{iT}\lambda_c/3 - st_c = 0 \dots \dots \dots (2.34)$$

Numerical solutions of eqn 2.34 show that the values of λ_{iT} are very nearly equal to $\sqrt{2\lambda_i}$ (λ_i being the constant momentum value of eqn 2.29) for a wide range of λ_c and is exactly equal to $\sqrt{2\lambda_i}$ for the hovering condition ($\lambda_c=0$).

Thus, when we assume the induced velocity is linear, which, as we have said, is good approximation to real conditions, v_{iT} can be replaced with good accuracy by $\sqrt{2\lambda_i}$. Substituting for λ_{iT} in

eqn 2.32 gives

$$t_c = \frac{a}{4} \left[\frac{2}{3} \left(\theta_0 - \frac{3}{4} \theta_1 \right) - \lambda_c - \frac{2\sqrt{2}}{3} \lambda_i \right] \text{--- --- (2.35)}$$

But $\theta_0 - (3/4)\theta_1$ is the blade pitch angle at $(3/4)R$ and $2\sqrt{2}/3 = 0.943$; hence, if we take θ_0 as the value of θ at the $3/4$ radial position and approximate $2\sqrt{2}/3$ by unity, we can use the simple equations 2.28 and 2.29 or 2.30 and 2.31 for all cases.

Thus, when we assume the induced velocity is linear, which, as we have said, is good approximation to real conditions, v_{IT} can be replaced with good accuracy by $\sqrt{2}\lambda_i$. Substituting for λ_{IT} in eqn 2.32 gives

$$t_c = \frac{a}{4} \left[\frac{2}{3} \left(\theta_0 - \frac{3}{4} \theta_1 \right) - \lambda_c - \frac{2\sqrt{2}}{3} \lambda_i \right] \text{--- --- (2.35)}$$

But $\theta_0 - (3/4)\theta_1$ is the blade pitch angle at $(3/4)R$ and $2\sqrt{2}/3 = 0.943$; hence, if we take θ_0 as the value of θ at the $3/4$ radial position and approximate $2\sqrt{2}/3$ by unity, we can use the simple equations 2.28 and 2.29 or 2.30 and 2.31 for all cases.

These approximations mean that the thrust will be underestimated by about 2 or 3 per cent relative to eqns 2.32 and 2.34, but, since the blade lift slope and the actual induced velocity will not be known precisely, further refinement is hardly justified.

It can easily be verified that if the blade planform also has linear taper, eqn 2.28 still holds, with the exception of some very small terms, if the chord is taken as that at $3/4 R$ as well as the blade pitch angle.

A useful relationship between the thrust coefficient and the blade lift coefficient can be obtained since, for constant blade chord,

$$\begin{aligned} T &= \frac{1}{2} \rho b c \Omega^2 R^3 \int_0^1 x^2 C_L dx \\ t_c &= \frac{1}{2} \int_0^1 x^2 C_L dx \\ &= \frac{\overline{C_L}}{3} \text{--- --- (2.36)} \end{aligned}$$

$$\overline{C_L} = 3 \int_0^1 x^2 C_L dx$$

If the lift coefficient is constant along the blade, then

$$t_c = C_T / s = C_L / 6$$

Usually the rotor operates at a mean CL of between 0.35 and 0.6, giving typical values of t_c within the range of 0.06 to 0.1. The rotor torque can be calculated in a similar way to the rotor thrust. From Fig. 2.11, the torque dQ of a blade element about the axis of rotation is

$$\begin{aligned} dQ &= r(dD + \phi dL) \\ &= (1/2)\rho \Omega^2 r^3 (\delta + \phi C_L) dr \end{aligned}$$

where δ is the local blade section drag coefficient. If δ is assumed to be constant, eqn 2.37 can be integrated to give

$$Q = \frac{\delta \rho b c \Omega^2 R^4}{8} + \frac{1}{2} \rho b c \Omega^2 R^4 \int_0^1 x^3 \phi C_L dx \quad \text{--- (2.38)}$$

Defining a torque coefficient q_c by

$$q_c = \frac{\delta}{8} + \frac{1}{2} \int_0^1 x^3 \phi C_L dx \quad \text{--- (2.39)}$$

Assuming constant induced velocity, $\phi = (\lambda_c + \lambda_i)/x$, so that eqn 2.39 becomes, on using eqn 2.36,

$$q_c = \delta/8 + (\lambda_c + \lambda_i)t \quad \text{--- (2.40)}$$

For the special case of hovering flight, $\lambda_c = 0$,

$$\begin{aligned} q_c &= \delta/8 + \lambda_i t_c \\ &= \frac{\delta}{8} + \sqrt{(s/2)t_c^2} \quad \text{--- (2.41)} \end{aligned}$$

Defining a torque coefficient q_c by

$$q_c = \frac{\delta}{8} + \frac{1}{2} \int_0^1 x^3 \phi C_L dx \quad \text{--- (2.39)}$$

Assuming constant induced velocity, $\phi = (\lambda_c + \lambda_i)/x$, so that eqn 2.39 becomes, on using eqn 2.36,

$$q_c = \delta/8 + (\lambda_c + \lambda_i)t \quad \text{--- (2.40)}$$

For the special case of hovering flight, $\lambda_c = 0$,

$$\begin{aligned} q_c &= \delta/8 + \lambda_i t_c \\ &= \frac{\delta}{8} + \sqrt{(s/2)t_c^2} \quad \text{--- (2.41)} \end{aligned}$$

The first term of eqn 2.41 represents the torque required to overcome the profile drag; the second represents the torque to overcome the induced drag of the blades.

It can be seen that the second term is the non-dimensional form of the hovering power calculated from energy and momentum considerations.

Using momentum principles we can find the effect of a non-uniform induced velocity distribution on the induced power. Let us assume that eqn of power in holds in differential form; then in hovering flight we can write

$$dP = dT v_i = 4 \pi r \rho v_i^3 dr$$

where v_i is the local induced velocity. If we take the linear induced velocity distribution $v_i = v_{iT} x$, we have

$$P = \frac{4\pi R^2 \rho v_{iT}^3}{5} \dots \dots (2.42) \quad dP = 4\pi R^2 \rho v_{iT}^3 x^4 dx$$

The thrust from momentum considerations is

$$T = 4\pi \rho R^2 \int_0^1 v_{iT}^2 x^3 dx$$

$$T = \rho \pi R^2 v_{iT}^2 \dots \dots \dots (2.43)$$

If the induced velocity v_i is constant, we have, for the corresponding thrust T_0 ,

$$T_0 = \rho \pi R^2 v_i^2 \dots \dots (2.44)$$

Comparing eqns 2.43 and 2.44 we see that for the thrusts to be the same we must have

$$v_{iT}^2 = 2v_i^2$$

Then

$$P = 8\sqrt{2} \rho \pi R^2 v_i^3 / 5$$

and, if P_0 is the induced power when the induced velocity is constant,

$$P_0 = 2 \rho \pi R^2 v_i^3$$

Hence

$$P/P_0 = 4\sqrt{2}/5 = 1.131$$

that is, when the induced velocity is linear, the induced power is about 13 per cent higher than if the induced velocity were constant; the latter condition corresponding to the least induced power for a given thrust. For the linear induced velocity, the torque coefficient would be

$$q_c = \delta/8 + 1.13\sqrt{(s/2)} t_c^{3/2} \dots \dots \dots (2.45)$$

A typical value assumed for δ is 0.012. With typical values of

0.05 and 0.08 for the solidity and thrust coefficient respectively, the two terms of q_c are 0.0015 and 0.00403, showing that the induced power is more than two and a half times the profile drag power.

Tests on aerofoils with rotor blade type of construction show that δ depends considerably on incidence and can be represented in the form and has used them in the calculation of thrust, H-force, and torque coefficients in hovering and vertical flight

$$\delta = \delta_0 + \delta_1\alpha + \delta_2\alpha^2 \dots \dots \dots (2.46)$$

Bailey has suggested the values

$$\delta = 0.0087 - 0.0216\alpha + 0.4\alpha^2 \quad (\alpha \text{ in radians})$$

The expressions which had to be calculated were very lengthy and the results were given in tabular form. They are to be found in the book by Gessow and Myers.

Since, however, Bailey used constant induced velocity in his calculations, it is rather doubtful whether the results he obtained would have been much better than if δ had been assumed constant because, in forward flight especially, the induced velocity differs considerably from the constant mean value, with correspondingly large variations in local blade incidence.

Another parameter of great importance is Mach number, especially for current helicopters which operate at higher tip speeds than formerly. With Mach number and induced velocity properly taken into account, the calculations of thrust and torque become more complicated; However, equations 2.28 and 2.45 give acceptable accuracy for many performance problems.

Calculation of the inflow angle

When making rotor calculations, it is often useful to know the inflow angle when the rotor geometry and operating conditions are given. We saw in the last section that the elementary thrust dT on an annulus of the rotor disc, when there are b blades, is

$$dT = \frac{1}{2} \rho abc \Omega^2 r^2 (\theta - \phi) dr \quad \dots \dots \dots (2.47)$$

where it has been supposed that the local lift coefficient is given by $C_L = a\alpha$

Now $\varphi = (V_c + v_i)/\Omega r$

so that eqn 2.47 can be written

$$dT = \frac{1}{2} \rho abc \Omega^2 r^2 (\theta - (V_c + v_i)/\Omega r) dr \quad \text{--- (2.47)}$$

Momentum theory applied to the annulus gives

$$dT = 4\pi\rho(V_c+v_i)v_i r dr$$

and on eliminating dT from eqn 2.48 we have

$$v_i^2 + \left(V_c + \frac{abc\Omega}{8\pi} \right) v_i - \frac{abc\Omega^2 r}{8\pi} \left(\theta - \frac{V_c}{\Omega r} \right) = 0 \quad \text{--- (2.49)}$$

Writing $\lambda_i = v_i/\Omega r$ and $\lambda_c = V_c/\Omega r$, as before, and putting $\sigma = bc/\pi r$, where σ is the solidity based on the local radius, eqn 2.49 becomes

$$\lambda_i^2 + \left(\lambda_c + \frac{a\sigma x}{8} \right) \lambda_i - \frac{a\sigma x}{8} \left(\theta - \frac{\lambda_c}{x} \right) = 0 \quad \text{--- (2.50)}$$

In eqn 2.50 σ and θ are variables, so that variable twist and taper can be taken into account. In hovering flight $\lambda_c = 0$ and eqn 2.50 reduces to

$$\lambda_i^2 + \left(\frac{a\sigma x}{8} \right) \lambda_i - \frac{a\sigma x}{8} (\theta) = 0 \quad \text{--- (2.51)}$$

Since $\varphi = v_i/\Omega r = \lambda_i/x$, eqn 2.51 can be written as

$$\phi^2 + \left(\frac{a\sigma}{8} \right) \phi - \frac{a\sigma}{8} (\theta) = 0$$

$$\phi^2 = \left(\frac{a\sigma}{8} \right) (\theta - \phi) = 0 \quad \text{--- (2.52)}$$

Hence, given the local blade pitch angle and solidity, the local value of φ can be calculated and then used in eqns 2.25 and 2.38 to obtain the thrust and torque.

Further, $\theta - \varphi$ is the local blade incidence and $a(\theta - \varphi)$ the local blade lift coefficient.

As an example of the use of eqn 2.52, let us consider a three-bladed rotor whose pitch angle at the blade root is 12° and whose blades have a washout* of 5° . The blade has a radius of 25 ft (7.6 m) and a constant chord of 1.5 ft (0.46 m). The lift slope of the blade section is assumed to be 5.7. Table 2.1 shows how the required quantities vary along the span, φ being obtained as the solution of eqn 2.52.

Table 2.1 Variation of ϕ , α and C_L with blade section radius

$x = r/R$	0.3	0.5	0.7	0.8	0.9	1
θ rad	0.178	0.158	0.136	0.126	0.115	0.105
σ	0.191	0.114	0.082	0.0715	0.0636	0.0573
ϕ	0.102	0.0795	0.0639	0.0585	0.0531	0.0483
$\alpha = (\theta - \phi)^\circ$	4.36	4.49	4.13	3.86	3.54	3.24
$C_L = a(\theta - \phi)$	0.434	0.447	0.411	0.385	0.353	0.324

* A twisted rotor blade or wing is said to have ‘washout’ when the incidence of the tip section is less than that of the root.

From eqn 2.36 it can be seen that we can calculate the thrust coefficient by the integration of $x^2 C_L$, which is proportional to the blade aerodynamic loading. The variation of $x^2 C_L$ along the blade span is shown in Fig. 2.12. On integration we find that $t_c = 0.0639$. Let us compare this value with the thrust coefficient calculated from eqns 2.30 and 2.31. Eliminating λ_i gives the following quadratic in t_c 1/2 :

$$t_c = (a/4)[2\theta_0/3 - \sqrt{(st_c/2)}] \text{ --- --- --- (2.53)}$$

and the pitch angle to be used is the value of θ at $3/4R$, i.e. 7.5° as discussed. Solving eqn 2.53, with $s = 0.0573$, gives $t_c = 0.0638$, which agrees extremely well with the previous result and shows that the simple analysis gives an accuracy well within that of the assumed value for the lift slope.

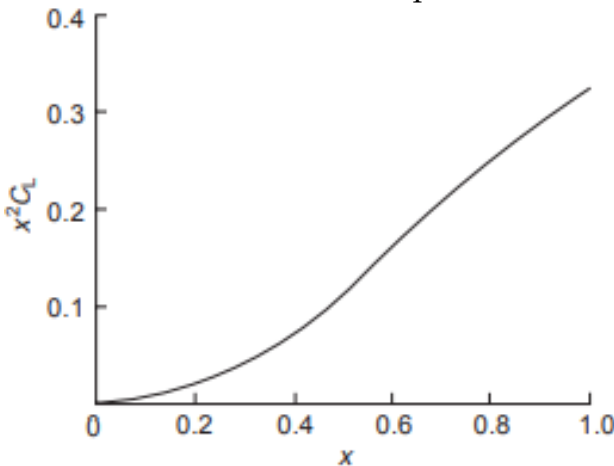


Figure 28. Non-dimensional blade loading as a function of span

VI. THE OPTIMUM ROTOR

It was stated in the blade element theorem section that the lowest induced power occurs when the induced velocity is

uniform over the disc.

The optimum rotor would be one designed so that this state was achieved and, in addition, the angle of attack would be chosen so that the section would be operating at the most efficient lift coefficient, which is not necessarily at the highest C_L/C_D ratio.

In hovering flight, the pitch angle of a blade element is

$$\begin{aligned} \theta &= \alpha + v_i/\Omega r \\ &= \alpha + \lambda_i/x \text{ --- --- (2.54)} \end{aligned}$$

where v_i is constant. The angle of attack α is also the constant value chosen as the most efficient. Thus the pitch angle can be considered as consisting of a constant part and a part which varies inversely with blade radius.

Now the thrust on an annulus of the rotor from the blade element theory is

$$dT = \frac{1}{2} \rho \Omega^2 r^2 a \alpha c dr$$

and from momentum theory

$$dT = 4 \pi \rho r v_i^2 dr$$

Equating these differential thrusts shows that to ensure constant induced velocity the chord must vary inversely with the radius. Thus, the optimum rotor must be twisted in accordance with eqn 2.54 and tapered inversely as the radius. The latter requirement would result in an unusual blade shape and one that would be difficult to construct.

Departures from the optimum blade, which usually means only that the chord is kept constant, do not result in a serious loss of efficiency; usually the amount is about 2 to 3 per cent more power for a given thrust. The subject is dealt with in some detail by Gessow and Myers. The reader is recommended to compare an optimum rotor with one of the same solidity having, say, constant chord and twist differing from the optimum.

The equivalent chord c_e of a rotor on a thrust basis is defined as

$$c_e = \frac{\int_0^1 cx^2 dx}{\int_0^1 x^2 dx}$$

$$c_e = 3 \int_0^1 cx^2 dx \text{ --- (2.55)}$$

and on a torque basis

$$c_e = 4 \int_0^1 cx^3 dx \text{ --- (2.56)}$$

These are the values of the chord for which constant-chord blades would yield the same thrust and torque as a tapered blade, for the same radius and incidence distribution.

The efficiency of a rotor

The efficiency of any device should indicate the measure of the success with which that device performs its duty. It is reasonable to want a hovering rotor to produce the most thrust for the least power; that is, to make the ratio T/P as large as possible.

This simple criterion has been objected to on the grounds that T/P is not a dimensionless quantity. The standard measure of efficiency adopted in helicopter work is the figure of merit M defined by

$$\bar{M} = \frac{TV_i}{P}$$

where v_i is the mean momentum induced velocity in hover. Since TV_i is the ideal induced power, the figure of merit is the ratio of the induced power to the total power. Since $P = TV_i + P_p$, where P_p is the profile drag power, the figure of merit can also be written as

$$\bar{M} = \frac{TV_i}{(TV_i + P_p)}$$

and, in non-dimensional form, as

$$\bar{M} = \sqrt{\left(\frac{S}{2}\right)} t_c^{3/2} / q_c$$

It could well be argued that the figure of merit so defined is even less satisfactory than the ratio T/P, because for constant thrust a high value can be achieved by increasing the induced velocity (by reducing the radius, say), thereby increasing the total power, which is the opposite of the desired effect.

A

$$\frac{T}{P} = \frac{T}{\frac{T^{3/2}}{\sqrt{(2\rho A)}} + \frac{\delta\rho s A \Omega^3 R^3}{8}} \quad \text{--- (2.57)}$$

The first term in the denominator of eqn 2.57 is the induced power, and the second term is the profile drag power.

Suppose the rotor radius is kept constant and the thrust is kept constant in such a way as to keep the incidence at a favourable value. This means that the mean lift coefficient and, hence, t_c is kept constant.

But since $T = t_c \rho s A \Omega^2 R^2$, we must have $s\Omega^2$ constant, so the only variable term in T/P is the profile drag power, which must therefore be proportional to Ω .

Thus T/P can be increased by reducing Ω , which also requires s to increase; or, in other words, we need a low rotor speed and high solidity if the radius is to be kept constant.

Suppose now we fix the thrust, solidity, and tip speed ΩR and vary the rotor radius. Differentiating eqn 2.57 with respect to A gives

$$\frac{\partial \left(\frac{T}{P} \right)}{\partial A} = T \frac{\frac{\delta\rho s \Omega^3 R^3}{8} - \frac{T}{2\sqrt{2}\rho A^{3/2}}}{\left[\frac{\delta\rho s \Omega^3 R^3}{8} - \frac{T^{3/2}}{\sqrt{2}\rho A} \right]^2} = 0$$

For Maximum T/P

i.e.

$$\frac{\delta\rho s \Omega^3 R^3}{8} = \frac{T}{2\sqrt{2}\rho A}$$

that is, the profile power is half the induced power for maximum T/P . The figure of merit for this condition is $2/3$.

Finally, for a given tip speed, solidity, disc area, and drag coefficient, we can write

$$\frac{T}{P} = \frac{1}{\Omega R} \frac{t_c}{\delta/8 + \sqrt{s/2} t_c^{3/2}}$$

$$\frac{\partial \left(\frac{T}{P} \right)}{\partial A} = T \frac{\frac{\delta \rho s \Omega^3 R^3}{8} - \frac{T}{2\sqrt{2}\rho A^{3/2}}}{\left[\frac{\delta \rho s \Omega^3 R^3}{8} - \frac{T^{3/2}}{\sqrt{2}\rho A} \right]^2} = 0$$

For Maximum T/P

i.e.

$$\frac{\delta \rho s \Omega^3 R^3}{8} = \frac{T}{2\sqrt{2}\rho A}$$

that is, the profile power is half the induced power for maximum T/P. The figure of merit for this condition is 2/3 . Finally, for a given tip speed, solidity, disc area, and drag coefficient, we can write

$$\frac{T}{P} = \frac{1}{\Omega R} \frac{t_c}{\delta/8 + \sqrt{s/2} t_c^{3/2}}$$

$$\frac{\partial \left(\frac{T}{P} \right)}{\partial t_c} = \frac{1}{\Omega R} \frac{\delta/8 + \sqrt{s/2} t_c^{3/2} - \frac{3}{2} t_c^{3/2} \sqrt{s/2}}{\delta/8 + \sqrt{s/2} t_c^{3/2}} = 0$$

Or

$$\frac{1}{2} \sqrt{s/2} t_c^{3/2} = \delta/8$$

and, as above, the profile power is half the induced power and the figure of merit is again 2/3 . If we take as typical values $s = 0.05$ and $\delta = 0.012$, we find the optimum value of t_c to be 0.072.



SATHYABAMA

**INSTITUTE OF SCIENCE AND TECHNOLOGY
(DEEMED TO BE UNIVERSITY)**

Accredited "A" Grade by NAAC | 12B Status by UGC | Approved by AICTE

www.sathyabama.ac.in

**SCHOOL OF MECHANICAL ENGINEERING
DEPARTMENT OF MECHANICAL ENGINEERING**

UNIT – III - POWER ESTIMATES – SAE1608

I. HELICOPTER PERFORMANCE IN FORWARD FLIGHT

It is now possible to estimate the performance of the helicopter in forward flight, this being the performance at a specific flight condition, or point on the flight envelope. This should not be confused with the mission performance, which is aimed at assessing the overall ability of the helicopter to complete a particular operational mission that consists of a series of inter-related tasks.

The trim calculations of the previous sections give all the information needed for calculating the power required for a given flight condition; in fact, using eqn 3.66, the torque and power were calculated from the values of θ_0 and λ was obtained from the trim equations. For the performance alone, however, calculation of the trim parameters is not necessary. A form of the torque equation for performance calculations more convenient than eqn 3.66 can be obtained by considering the balance of forces along the flight path in conjunction with eqn 3.66.

Referring to Fig. 30, we see that

$$T_D \sin \alpha_D + H_D \cos \alpha_D + W \sin \tau_c + D = 0$$

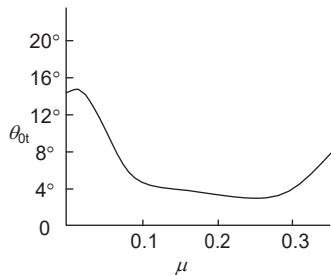


Fig. 30 Tailrotor pitch angle to trim

Multiplying by $\hat{V} = V/\Omega R$ and remembering that $\hat{V} \sin \alpha_D = \lambda_D + \lambda_i$ gives

$$(\lambda_D + \lambda_i)T_D + \mu H_D + W\hat{V} \sin \tau_c + D\hat{V} = 0$$

which can be written in non-dimensional form as

$$\lambda_D t_{cD} + \mu h_{cD} = -(\lambda_i t_{cD} + w_c \hat{V} \sin \tau_c + \frac{1}{2} \hat{V}^3 d_0)$$

Substituting for $\lambda_D t_{cD} + \mu h_{cD}$ in eqn 3.66 gives

$$q_c = \delta(1 + 3\mu^2)/8 + \lambda_i t_{cD} + w_c \hat{V} \sin \tau_c + \frac{1}{2} \hat{V}^3 d_0 \quad (4.19)$$

This expression for the torque coefficient can be regarded as the non-dimensional form of an energy equation; the first term represents the power required to overcome the profile drag of the blades, the second represents the induced power, the third is the power required for climbing, and the last term is the power required to overcome the fuselage drag. Of course, eqn 4.19 could have been derived from energy considerations directly, but it is instructive to derive it from the balance of forces.

Equation 4.19 has been derived from eqn 3.66 on the assumption that the induced velocity was constant. Since the induced power in eqn 4.19 appears as a separate term, it is a simple matter to include the effect of non-uniform induced velocity, as mentioned in the previous chapter. Now, as we saw in Chapter 3, the induced power can be expressed as $(1 + k)P_{i0}$, where P_{i0} is the 'ideal' induced power for a constant induced velocity distribution defined by $v_{i0}T$ and which, in non-dimensional form, is represented by the second term of eqn 4.19. Values of k for the Mangler and Squire induced velocity distribution were given in Fig. 3.16.

Thus, the contribution of the induced power to the torque coefficient can be expressed more accurately by $(1 + k)\lambda_i t_{c_i}$. Further, we have yet to include the torque which must be provided to the tailrotor. The tailrotor is driven by a shaft geared to the main rotor, but the torque supplied to the shaft depends on the inclination of the tailrotor axis to the fuselage. Thus, for example, it is possible to incline the axis so that the tailrotor autorotates and for no power to be necessary at the tailrotor, causing a drag force which, in turn, would require a forward tilt of the main rotor to trim it, with a corresponding increase of power to be developed at the main rotor shaft.

It can easily be verified that the amount of power required at the tailrotor shaft, plus the work which must be done to overcome the tailrotor force, is independent of the tailrotor shaft angle. As we have found with the main rotor, the power absorbed can be expressed simply as that which would be needed to overcome the profile drag of the blades and the induced power. Hence, the power P_t required for the tailrotor is

$$P_t = \left[\frac{\delta_1}{8}(1 + 3\mu_1^2) + \lambda_{it} t_{ct} \right] \rho s_1 A_1 (\Omega R)_1^3$$

and the effective increment to the mainrotor torque coefficient is

$$q_{ct} = \left[\frac{\delta_1}{8}(1 + 3\mu_1^2) + \lambda_{it} t_{ct} \right] \frac{s_1 A_1 (\Omega R)_1^2}{s A (\Omega R)^3}$$

Now it is reasonable to assume that, as the tip speeds of the tailrotor and the main rotor are usually equal, the terms in the square bracket have roughly the same values as those of the main rotor, although, as we saw earlier, λ_{it} may be rather higher than in hovering flight. Hence, the power to be attributed to the tailrotor is, to a good approximation, $s_t A_t / s A$ times that of the main rotor. Thus, a simple way to calculate the tailrotor power is merely to increase the mainrotor power by the fraction $s_t A_t / s A$ whose value is typically about 0.06. As a percentage of the *total* power, the tailrotor power varies from about 6 per cent in hovering to about 3 per cent at high speed.

The torque coefficient can finally be written as

$$q_c = \left[\frac{\delta}{8} (1 + 3\mu^2) + (1 + k)\lambda_i t_{cd} \right] \left(1 + \frac{s_t A_t}{s A} \right) + w_c \hat{V} \sin \tau_c + \frac{1}{2} \hat{V}^3 d_0 \quad (4.20)$$

The required power P is calculated from $\Omega Q = q_c \rho s A \Omega^3 R^3$ and is shown for the example helicopter in level flight in Fig. 30. The four contributions to the power are shown by the broken lines, the value of the induced power factor k being taken as 0.17. Suppose the maximum installed power of our example helicopter is 900 kW. It can be seen from Fig. 4.14 that the maximum excess power occurs at $\mu = 0.154$ (32 m/s) and is 496 kW. This gives a maximum rate of climb of 11 m/s. The maximum forward speed occurs when the installed power and the required power are equal; the intersection of the two curves in Fig. 31. occurs at $\mu = 0.358$, i.e. at 74.8 m/s.

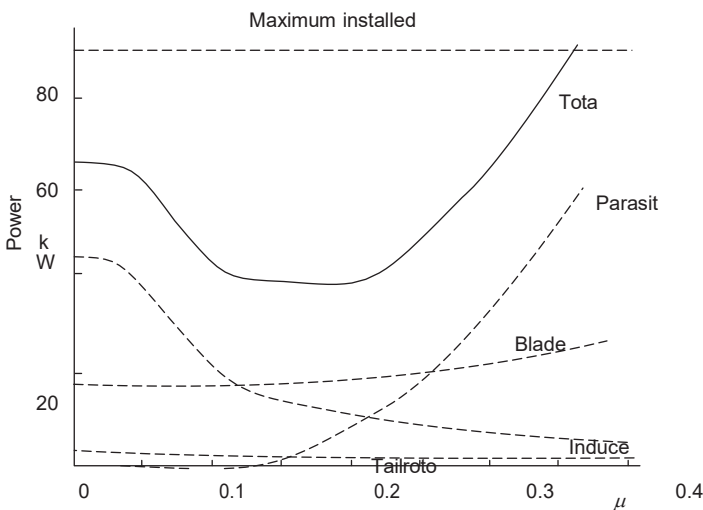


Fig. 31 Variation of power with forward speed

II. FUSELAGE PARASITE DRAG

The figure for the parasite drag of our example helicopter is a value, typical for its weight, of production helicopters. The flat plate parasite drag of a number of helicopters as a plot of equivalent flat plate area is shown against gross weight in Fig. 32. The points define fairly well a typical curve of drag against weight. A second curve is shown which is based on aerodynamically clean experimental helicopters. This latter curve represents the lowest drag which can reasonably be achieved in helicopter design, although it falls far short of best fixed wing practice. It is clear that the particular basic shape which must be adopted by helicopter fuselages, and the fact that the helicopter is normally expected to fulfil a variety of roles, means that it is unable to reach the degree of aerodynamic refinement which is possible in fixed wing practice. In fact, both helicopter drag curves are roughly proportional to $W^{1/2}$, instead of $W^{2/3}$ as might have been expected, which is an indication of a large amount of separation drag. The drag curve of the much cleaner fixed wing aircraft is more nearly proportional to $W^{2/3}$.

A breakdown of the fuselage parasite drag is shown in the table below.

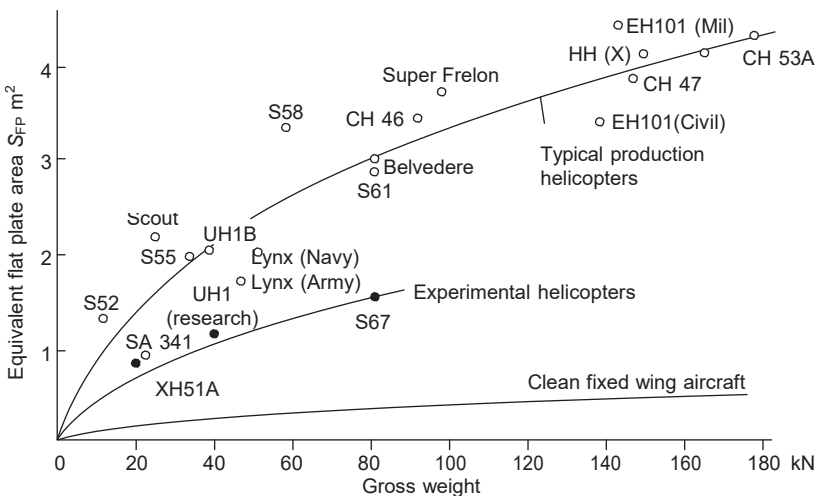


Fig. 32 Parasite drag of helicopters

<i>Component</i>	<i>Percentage drag</i>
Basic fuselage with protuberances	20 to 40
Landing gear or fairing	6 to 25
Rotor pylon and hub	35 to 50
Tailrotor and tail surfaces	5 to 15

The drag of the rotor pylon and hub represents a high proportion of the overall drag, and this is therefore an area where drag reduction leads to considerable benefit; hence the appearance of hub and pylon fairings on the larger and faster helicopters.

Interference drag plays a significant role, because on a helicopter there are a number of separate aerodynamic ‘shapes’ in close proximity whose pressure distributions and boundary layers can interact with each other. Hub and pylon fairings are designed to minimise interference drag in addition to reducing the basic parasitic drag contribution of these components, the upper cambered shape of the former being a result³.

Also, larger and faster helicopters tend to utilise retractable landing gear, which leads to the lower figure in the above table.

III. ANALYTICAL ESTIMATION OF PERFORMANCE

Except at very low speeds (when the disc incidence may not always be small) we can put $\lambda_i = \mu$ and $\lambda_i = st_c/2\mu$; also, writing λ_c for $\sin \tau_c$, eqn 4.20 can be expressed

as

$$q_c = \left[\frac{\delta}{8}(1 + 3\mu^2) + \frac{1}{2}(1 + k) \frac{st_c^2}{\mu} \right] \left(1 + \frac{s_t A_t}{sA} \right) + \lambda_c t_c + \frac{1}{2} \mu^3 d_0 \quad (4.21)$$

where q_c is the torque coefficient corresponding to the given power.

The expression for q_c can be used to calculate either the torque and power for a given flight condition or, as described below, the maximum speed and rate of climb for a given torque.

To find the maximum level speed ($\lambda_c = 0$) for a given power, i.e. given q_c , we have to solve the quartic in μ expressed by eqn 4.21. Now at high speed we note that the induced power is small; therefore, neglecting this term and the term $3\mu^2$ of the profile drag, we find as a first approximation to μ , μ_1 say

$$\mu_1^3 = \frac{2[q_c - \delta(1 + s_1 A_t / sA)]/8}{d_0}$$

The value of q_c corresponding to the maximum power (900 kW) is 0.00834. Then, with the previously given values of δ and d_0 , we find

$$\mu_1^3 = 0.0561 \quad \text{or} \quad \mu_1 = 0.383$$

With this value of μ , we calculate the terms previously neglected to give the second approximation μ_2 as

$$\mu_2^3 = 0.0468 \quad \text{or} \quad \mu_2 = 0.36$$

which is extremely close to the correct value. Thus, the iteration provides the required maximum value in two steps.

To find the maximum rate of climb we must satisfy the condition

$$\partial \lambda_c / \partial \mu = 0$$

This condition leads to

$$6d_0\mu^4 + [3\delta\mu^3 - 2(1+k)st_c^2] \left(1 + \frac{s_1 A_t}{sA}\right) = 0 \quad (4.22)$$

To solve this equation for μ we note from Fig. 4.14 that the blade profile drag contributes little to the slope of the power curve (which led to eqn 4.22), so that for a first approximation μ_1 we can neglect the second term of eqn 4.22 and obtain

$$\mu_1^4 = \frac{(1+k)st_c^2}{3d_0} \left(1 + \frac{s_1 A_t}{sA}\right)$$

$$\mu_1^4 = 0.000642$$

or

$$\mu_1 = 0.159$$

For the second approximation, a value for the second term is calculated using μ_1 , giving

$$\mu_2^4 = 0.000642 - 0.000117 = 0.000525$$

or

$$\mu_2 = 0.152$$

This agrees with the value obtained graphically and, again, the iteration leads to a satisfactory answer in two steps. This value of μ is substituted into eqn 4.21 and the equation is solved for λ_c , giving the required rate

of climb.

IV. AUTOROTATIVE FORWARD FLIGHT

Autorotation is defined as self-sustained rotation of the rotor in the absence of applied torque, i.e. when $Q = q_c = 0$. The work to be done to overcome the rotor and fuselage drag must be obtained at the expense of the potential energy of the helicopter. Level flight autorotation is impossible, and steady flight can be achieved only by descending. To find the rate of descent at a given forward speed we simply put $q_c = 0$ in eqn 4.21 and solve for λ_c at the appropriate value of μ . Thus

$$\lambda_c = - \frac{\delta}{8t_c} (1 + 3\mu^2) + \frac{1}{2}(1 + k) \frac{st}{\mu} + \frac{1}{2}\mu^3 \frac{d}{t_c} \quad (4.23)$$

and the rate of descent V_{des} is given by

$$V_{des} = - \lambda_c \Omega R$$

The angle of descent τ_{des} is clearly

$$\tau_{des} = \tan^{-1} (V_{des}/V) \quad (4.24)$$

The rate and angle of descent of our example helicopter is shown in Figs 33 and 34.

It can be seen from eqns 4.21 and 4.23 that the rate of descent is proportional to the torque coefficient in level flight; in fact, the rate of descent curve, Fig. 34, is

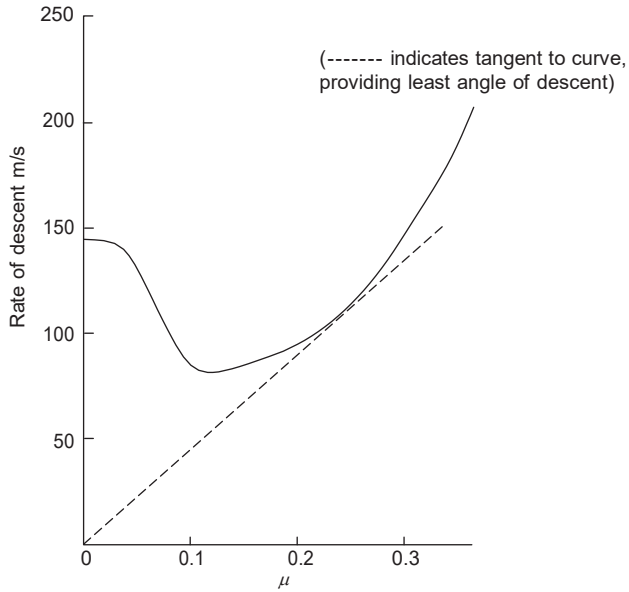


Fig. 33 Rate of descent in autorotation

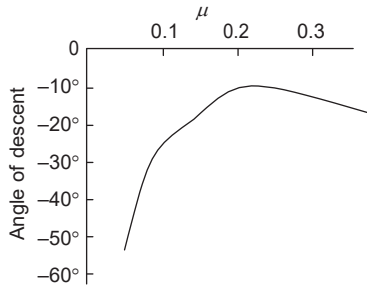


Fig. 34 Angle of descent in autorotation

merely the power curve, Fig. 34, drawn to a different scale. Thus, the minimum rate of descent occurs at the same speed as the minimum power in level flight.

From eqn 4.24 the condition for least angle of descent is given by

$$\frac{d\tau_{des}}{dV} = \frac{\cos^2 \tau_{des}}{V^2} \left(V \frac{dV_{des}}{dV} - V_{des} \right) = 0$$

i.e.
$$dV_{des}/dV = V_{des}/V$$

Except at low speeds, when the disc angle may be quite large, this condition can be written as

$$d\lambda_c/d\mu = \lambda_c/\mu$$

and the solution can be found by the point at which the line drawn from the origin makes a tangent to the curve of λ_c against μ or of V_{des} against μ , as shown in Fig. 4.16.

In autorotation there must be a flow up through the rotor disc so that the total moment, or torque, of the blade forces is zero. Figure 4.18 shows the forces on a blade section with the resultant force dR perpendicular, or nearly perpendicular, to the plane of rotation. It can be seen that the resultant velocity vector W must be inclined upwards relative to the plane of rotation in order that there should be a component of lift to balance the blade drag.

It is clear that in autorotation the collective pitch will be lower than in forward flight. To find the collective pitch angle to trim it is best to use eqn 3.66, putting $q_c = 0$ and neglecting the small term in $\mu h_c D$, giving

$$\lambda_D = \delta(1 + 3\mu^2)/8t_{cD} \tag{4.25}$$

Since $t_{cD} = w_c$, λ_D can easily be calculated from eqn 4.25 and then substituted in eqn 3.63 to obtain θ_0 . The collective pitch variation with μ is shown in Fig. 4.19. The fact that it is practically constant follows from the need for an almost constant flow through the rotor to maintain zero torque, as can be seen from an inspection of eqn 4.25.

i. GENERAL REMARKS ON PERFORMANCE ESTIMATION

The performance estimations discussed in this chapter have been based on very simple assumptions, particularly with regard to the aerodynamic properties of the

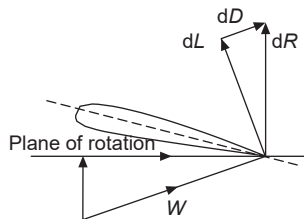


Fig. 35 Forces on aerofoil in autorotation

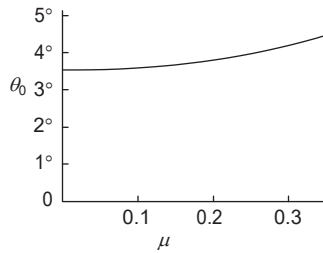


Fig. 36 Collective pitch to trim in autorotation

blades. One of the most important, and which has allowed a particularly simple analysis, is the assumption of constant blade section drag coefficient even though, as we shall discuss in detail in Chapter 6, the local incidence may vary over a wide range and enter the stall region.

An early attempt to consider the dependence of the drag coefficient δ on the incidence α was that of Bailey (1941)⁴, who assumed that

$$\delta = 0.0087 - 0.0216\alpha + 0.4\alpha^2$$

This expression was inserted into the same sort of analysis as presented in Chapter 3, using a tip loss factor $B = 0.97$, $\gamma = 15$, and an arbitrary amount of linear twist. The induced velocity was assumed to be constant.

As might be expected, the expressions for the force, torque, and flapping coefficients were quite complicated, partly on account of the presence of the tip-loss factor B .

For performance estimation, Bailey and Gustafson⁵ calculated the induced, fuselage,

and tailrotor power contributions in a manner similar to that described in this chapter, but for the profile power Bailey's results were used by expressing them in chart form for zero blade twist. However, in order to use the charts it was still necessary to find the trim values of θ_0 and λ and also to interpolate between charts. Although Bailey's analysis would appear to contain a more accurate representation of the blade drag, it is doubtful if it justifies the extra complexity or even gives a more reliable value of the profile power; for example, the inclusion of the tip loss factor leads to many terms in B^4 and B^5 so that a bad choice of the value of B can clearly make a considerable difference to the final result. In any case, the value of B normally assumed is based on hovering flight theory and is not applicable to forward flight.

This illustrates the case against too great an expenditure of effort in estimating the performance of the rotor, as can be seen also by referring to Fig. 4.20. The figure shows the effective L/D ratio of the complete helicopter plotted against the L/D ratio

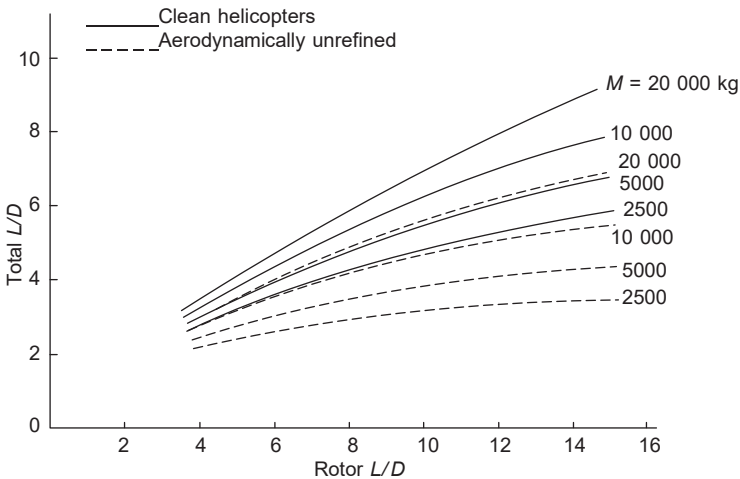


Fig. 37 Effect of L/D of rotor on L/D of complete helicopter

of the rotor alone. The effective drag has been calculated from the power expended, P , by

$$D = P/V$$

giving

$$L/D = VW/P = VW/(P_p + P_i + P_t + P_f)$$

where P_p , P_i , P_t , and P_f are, respectively, the blade profile drag and the induced, tailrotor, and fuselage power contributions.

At cruising speeds, i.e. for tip speed ratios of between, say, 0.25 and 0.35, it can be calculated from the data of Fig. 4.14 that the L/D ratio

for the rotor alone of our example helicopter varies from about 7 to 10. Figure 4.20 shows that, at these values, a comparatively large increase of the L/D ratio of the rotor would be needed to produce a significant increase in the L/D ratio of the complete helicopter, especially at low values of the gross weight.

Thus, there is a limit to the expenditure of effort that ought reasonably to be spent in either making calculations of the rotor power or effecting real improvements in rotor performance through aerodynamic refinement.

What has been said above applies strictly to the calculation of the *performance* of the helicopter, by which we mean the estimation of the power for a given flight condition or the flight range possible for a given installed power. The high speed performance of modern helicopters, however, is far more likely to be restricted by the vibration and increase of control loads due to blade stall and compressibility than through lack of power. It is in this area that the aerodynamics of the rotor must be considered in sufficient detail to be able to design a rotor in which these undesirable effects are reduced to a minimum



SATHYABAMA

INSTITUTE OF SCIENCE AND TECHNOLOGY
(DEEMED TO BE UNIVERSITY)

Accredited "A" Grade by NAAC | 12B Status by UGC | Approved by AICTE

www.sathyabama.ac.in

SCHOOL OF MECHANICAL ENGINEERING

DEPARTMENT OF AERONAUTICAL ENGINEERING

UNIT – IV– LIFT, PROPULSION AND CONTROL OF V/STOL AIRCRAFT – SAE1608

I. INTRODUCTION

The abbreviation V/STOL is a combination of two other abbreviations, VTOL and STOL, which stand for “vertical take-off and landing” and “short take-off and landing.” Thus V/STOL aerodynamics refers to an area of the subject of aerodynamics that is of special interest to the design of aircraft with vertical take-off and landing or short take-off and landing capabilities.

V/STOL aerodynamics is concerned primarily with the production of lift at low forward velocities. There is a qualification to the production of this lift, however. It is not to be accomplished at a sacrifice in the cruising performance of the aircraft. Hence an aircraft with low take-off and landing speeds because of low wing loading would not, in general, be termed a “short take-off and landing” aircraft. A vertical or short take-off and landing aircraft employs some special kind of device to produce lift at low speeds. Here, the term “lift” is used in a general sense to denote the vertical force that sustains the aircraft in flight. It might be composed of the usual lift from a lifting surface and a force produced by some form of propulsor.

It has been axiomatic in the gradual development of aircraft that their landing speeds and distances have increased in proportion to their cruising speeds. The requirement for longer and longer runways is in direct conflict with the growth of metropolitan areas. The need for a type of aircraft with exceptional take-off and landing performance is apparent. The logistics of modern warfare also require aircraft that can operate from small prepared or unprepared fields.

The development of such aircraft has proceeded rapidly with the introduction of suitable power plants. In particular, the gas turbine, with its low specific weight, that is, pounds of engine weight per pound of static thrust, has made possible the development of aircraft with static thrust to gross weight ratios greater than one. As the speeds of aircraft continue to increase, the power plant requirements for V/STOL operation and forward flight performance become compatible. Above Mach 1 the thrust required is nearly equal to or exceeds the gross weight of the aircraft. However, for sub-sonic aircraft the installed thrust needed for V/STOL performance normally exceeds that required for efficient cruise. For these applications, therefore, the aerodynamicist must consider means of improving the cruise performance.

The many convincing arguments that can be put forward in favor of the **VTOL** aircraft are based mainly on the removal of equipment and facilities that are required to accomplish the conventional landing. These include the conventional landing gear, with its array of mechanical, hydraulic, electrical, and pneumatic devices, and high-lift devices such as flaps, slats, and boundary layer control. The modern high-performance, conventional jet aircraft landing at speeds of the order of 150 to 200 knots requires runways in the 10,000-ft class. The problems of acquiring and maintaining such facilities and of braking the aircraft landing at these high speeds can be circumvented by the application of STOL and VTOL principles.

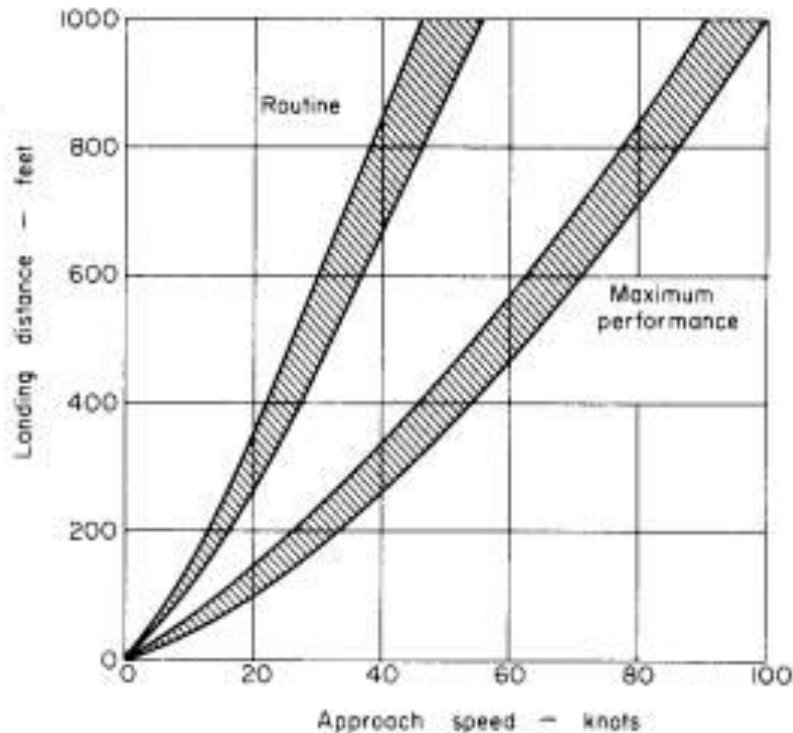


Figure 38. STOL Landing Performance

Investigators in the field differ in their opinions of an exact definition of a STOL aircraft. Most of them agree qualitatively on the characteristics a STOL aircraft must possess. It must be capable of takeoff and landing in a prescribed distance over a standard obstacle height, and the ratio of cruise speed to landing speed must be above a prescribed minimum. To fill these requirements simultaneously a STOL aircraft must possess some special design feature that will allow the development of lift at low speeds in excess of that developed by an ordinary wing.

A height frequently specified in takeoff and landing calculations is 50 ft. The horizontal distance to clear this obstacle height for STOL aircraft has been specified for some applications as 500 ft. However, this distance, as well as the ratio of cruising speed to landing speed, is not as well defined as the obstacle height. The reason is apparent, a turbojet fighter aircraft that might have a speed ratio of 20 and land in 1500 ft could be considered just as much of a STOL aircraft as a short-haul transport that can land in 500 ft but might have a speed ratio of only 6 or 7.

Consider the landing capabilities of STOL aircraft as shown in Fig. 1-1. This figure is derived from consideration of human response times obtained from actual flight tests with helicopters which showed that rates of descent of 500 to 700 fpm were the maximum that could be used with consistency. These limitations were derived from instrument approaches at altitude but are comparable to the highest rates of descent that can be used in the last 50 ft of altitude in an approach.

From this figure it can be seen that to land in 500 ft as a matter of routine requires an approach speed of approximately 30 knots. This assumes a rate of descent of 500 fpm, a circular arc transition with a normal acceleration of 0.1 g, and a stopping deceleration of 0.3

g. By the use of maximum techniques this approach speed can be increased to approximately 60 knots, which assumes a 1000-fpm rate of descent with no transition and a deceleration of 0.8 g. These assumptions are certainly on the optimistic side, and it would appear that the 30-knot approach speed is more realistic. In actual practice, however, the performance will probably be somewhere between these two extremes. The landing gear might be designed to withstand a rate of descent of approximately 700 to 800 fpm, and by reversing the propellers or thrust the deceleration could be increased to 0.5 or 0.6 g. Therefore an approach speed of 45 knots is representative of a STOL aircraft that would satisfy the landing requirement of 500 ft over a 50-ft obstacle. For example, one STOL reconnaissance aircraft, operational at the time of this writing, has a guaranteed landing distance over 50 ft of 775 ft for a stalling speed of 55 knots.

Additional insight into the factors influencing the takeoff or landing performance of an aircraft can be gained by a simplified analysis of the ground-roll distance of a landing aircraft. If T_R is the reverse thrust, μ , the coefficient of braking friction, W , the weight of the aircraft, and V , the velocity at time t , then the equation of motion of the aircraft is

$$\Sigma F = \frac{W}{g} \frac{dV}{dt}$$

or

$$-(T_R + \mu W) = \frac{W}{g} V \frac{dV}{ds}$$

This equation integrates to

$$\left(\frac{T_R}{W} + \mu\right) Ws = \frac{WV_0^2}{2g} - \frac{WV^2}{2g};$$

V_0 is the initial velocity of the aircraft in the s -direction at touchdown. The distance S_0 required for the aircraft to come to rest is found from

$$\left(\frac{T_R}{W} + \mu\right) WS_0 = \frac{W}{g} \frac{V_0^2}{2}$$

This equation assumes that T_R is a constant and neglects any lift produced during the ground roll. It shows that the work performed by the retarding forces must equal the initial kinetic energy of the aircraft. It also clearly illustrates the importance of keeping V_0 as small as possible, for the ground-roll distance S_0 varies as the square of V_0 .

If V_0 is taken to be 20% higher than the stalling speed, the distance S can be written as

$$S_0 = \frac{1.44(W/S)}{\rho g C_{L_{max}}(T_R/W + \mu)}$$

T_R is normally a function of the installed forward thrust. Because cruising requirements usually determine the thrust and the wing loading, it follows that the principal parameter in determining the landing distance, and the one over which the most control can be exercised, is the maximum lift coefficient. From this simplified analysis it can be seen that the landing distance might be expected to vary inversely with $C_{L_{max}}$.

Types of V/STOL Aircraft

There have been many schemes proposed for the design of STOL and VTOL aircraft. In VTOL aircraft, as in STOL aircraft, it is necessary to impose a minimum speed restriction. Thus a VTOL aircraft is defined as an aircraft with vertical takeoff and landing capabilities and cruising speeds equal to those of ordinary fixed-wing aircraft that perform comparable missions but from longer fields. This comparison with ordinary fixed-wing aircraft could apply as well to STOL aircraft in which the VTOL capability has been replaced by the takeoff and landing distance of 500 ft over a 50-ft obstacle.

In view of the speed requirement, helicopters and autogyros technically cannot be considered VTOL or STOL aircraft. The forward speed of the usual rotary-wing aircraft is limited by the conflicting requirements of compressibility effects and retreating blade stall. At the higher forward speeds it is desirable to run at a high rotor rpm because of retreating blade stall, but, conversely, it is desirable to run at a lower rpm to avoid compressibility effects on the rotor. Listed below are different types of **V/STOL** aircraft or methods of accomplishing V/STOL performance. Most of these topics are covered in detail in later chapters.

COMPOUND AIRCRAFT

A compound aircraft is a combination of helicopter and fixed-wing aircraft. In forward flight the lift is transferred to the Wing, thereby unloading the rotor. Forward thrust is provided by a propeller or a jet. In forward flight the rotor is allowed to autorotate or can be stopped and retracted into the fuselage. This type of aircraft is shown in Fig. 39.



Figure 39. A compound aircraft.

TAIL SITTERS

A tail sitter is an aircraft, either jet or propeller-driven, of rather conventional outward appearance but with enough thrust and appropriate controls to allow it to hover with the airplane axis in a vertical attitude. The coleopter, which is a ring-wing ducting a fan, also falls in this category.

TILT-RING

A tilt-wing aircraft derives **its** high lift by **rotating** the entire wing and propellers, mounted on the wing, through approximately 90° while keeping the fuselage horizontal. The major portion of the wing, submerged in the propeller slipstream, does not stall throughout a major part of the flight regime. The Vertol 76, shown in Fig.40, a flying test bed, was the first successful aircraft of this type to undergo transition.



Figure 40. The first successful tilt- wing aircraft, the Vertol 76. (Vertol Div., The Boeing Co)

TILTING JETS. DUCTED PROPELLERS, OR ROTORS

These three types are given together because the principle of rotating the thrust producer, is the same for each of them. They vary only in the degree of their disk loadings, hence in their jet velocities. For this type of aircraft only the thrust producer rotates; the aircraft fuselage and wing remains horizontal. The rotating thrust producers can be attached to the fuselage or mounted at the wing tips as shown in Fig. 41.



Figure 41. The Bell XV-3, a tilting-rotor VTOL aircraft. (Textron's Bell Helicopter Co.)

DEFLECTED UPSTREAM (VECTOREO SLIPSTREAM)

In a deflected slipstream system lift is produced at low speed by deflecting the propeller slipstream downward in a wing-flap system. The earliest of what might be termed STOL aircraft, the Crouch-Bolas Dragonfly I, flown in 1934, operated on this principle. Two opposite-rotating 9-ft-diameter propellers powered with 90 hp engines gave this 2100-lb, 26-ft span biplane exceptional short-field performance. It had a ground run of 30 ft, an angle of climb of 70° , and an angle of descent of 70° . Descent was made nose high with power [2].

DEFLECTED JET

The deflected jet principle is similar to the deflected slipstream, except that the turning is done internally. In hovering flight the exhaust from the turbojet engine, normally expelled in the aft direction, is diverted by a system of vanes to produce a vertical component of thrust.

EXTERNAL FLOW, JET-AUGMENTED FLAPS

The question might be asked, "When does a deflected slipstream or jet become an external flow, jet-augmented flap?" This is a little difficult to answer. However, in a deflected slipstream most of the lift is derived from redirecting the jet momentum, whereas in the externally augmented flaps increased lift is produced by the wing by means of circulation and boundary layer controls afforded by blowing over the flap.

BOUNDARY LAYER CONTROL (BLC)

There are several methods of boundary layer control, each of which has the same purpose of preventing boundary layer separation. One method controls the boundary layer by sucking off the slower-moving air either by a relatively uniform distribution of holes [3] or in a series of slots running spanwise along the airfoil [4].

Another method [5] feeds higher-energy air into the boundary layer by blowing air tangentially to the upper surface of a deflected flap. This scheme is sometimes referred to as a blown flap. It is also possible to accomplish BLC by means of a jet flap, which is simply a sheet of air blown downward from the trailing edge of an airfoil. Its effect on the airfoil is similar to that of the usual flap. In addition to blowing on trailing edge flaps, it is also possible to blow on leading edge flaps to prevent leading edge separation. These schemes are shown in Fig. 42.

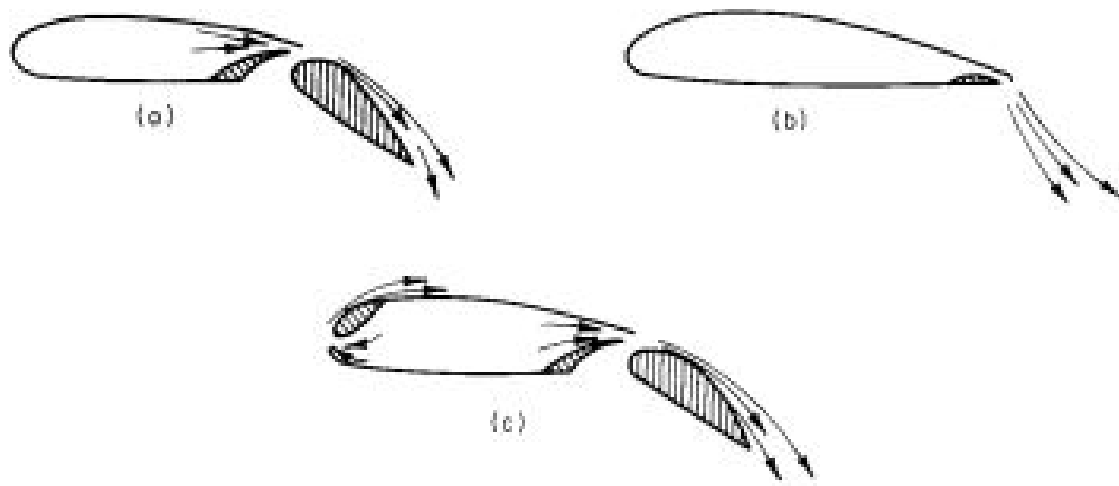


Figure 42. (a) Blown physical flap; (b) jet flap; (c) leading-and trailing-edge blowing.

CIRCULATION CONTROL

If the amount of air of a blown or jet flap is increased beyond the value required to prevent boundary layer separation, additional circulation is produced around the airfoil. This increased circulation will produce a lift in excess of that predicted from potential flow or jet reaction.

SUBMERGED FANS. LAN-IN-WING

In this configuration a large fan is submerged horizontally in the wing. In hovering the wing acts as a duct around the fan to improve its static thrust performance. In forward flight at low speeds the action of the fan is beneficial to the wing. An example of an aircraft incorporating this method of obtaining VTOL performances is illustrated in Fig. 43.



Figure 43. A fan-in-wing aircraft

DIRECT THRUST

In this scheme separate jet engines are nested in the wing or fuselage to provide vertical thrust. Although the flow over the wing is affected to some extent by the engines, the effect is limited so that the characteristics of this type of VTOL or STOL aircraft can be approximated by determining the behavior of the wing and engines separately.

AERODYNES, DUCTED FANS, AND HIGHLY LOADED ROTORS WITHOUT FIXED LIFTING SURFACES

These types of STOL or VTOL aircraft employ highly loaded rotors to provide the lift and thrust for forward flight. Control is accomplished either by tilting the axis of the rotor or by deflecting its slipstream with a system of vanes submerged in the rotor slipstream. Vehicles of this type include the “flying jeep” and the “aerodyne”.

THRUST AUGMENTATION

Somewhat similar to the jet pump, this configuration uses the primary flow from jets to induce a secondary flow. The static thrust available from a jet engine is therefore increased significantly by the entrained flow.

To summarize, many schemes have been proposed and are being studied for accomplishing STOL and VTOL aircraft.

1. Compound aircraft
2. Tail-sitters
3. Tilt-wing
4. Tilting-jets, ducted propellers or rotors
5. Deflected slipstream
6. Deflected jet
7. External flow, jet-augmented flaps
8. Boundary layer control
9. Circulation control

10. Submerged fans
11. Direct thrust
12. Aerodynes, ducted fans, and highly loaded rotors without fixed lifting surfaces
13. Thrust augmentation

These categories tend to overlap somewhat in their definitions. It is also possible that a V/STOL aircraft might incorporate several of these schemes to develop lift at low forward speed.



SATHYABAMA

INSTITUTE OF SCIENCE AND TECHNOLOGY
(DEEMED TO BE UNIVERSITY)

Accredited "A" Grade by NAAC | 12B Status by UGC | Approved by AICTE

www.sathyabama.ac.in

SCHOOL OF MECHANICAL ENGINEERING
DEPARTMENT OF AERONAUTICAL ENGINEERING

UNIT – V – GROUND EFFECT MACHINES – SAE1608

I. INTRODUCTION TO GROUND-EFFECT MACHINES

Although ground-effect machines (GEM) might be described as VTOL aircraft that never quite made it, they are believed to have sufficient potential to warrant at least a chapter. As the name implies, a GEM is limited to operating in proximity to a surface either a solid surface or over water. By so doing, however, it is able to sustain much greater loads for a *given* power than an aircraft that operates out of ground effect.

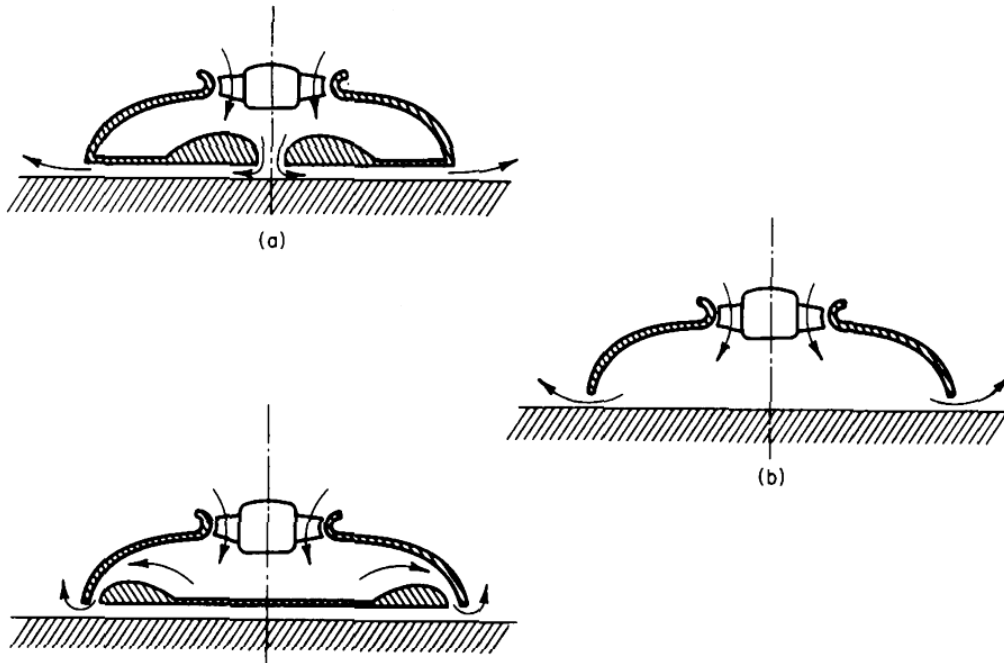


Figure. 44. Types of GEM's (a) Air bearing (b) Plenum Chamber (c) Peripheral jet

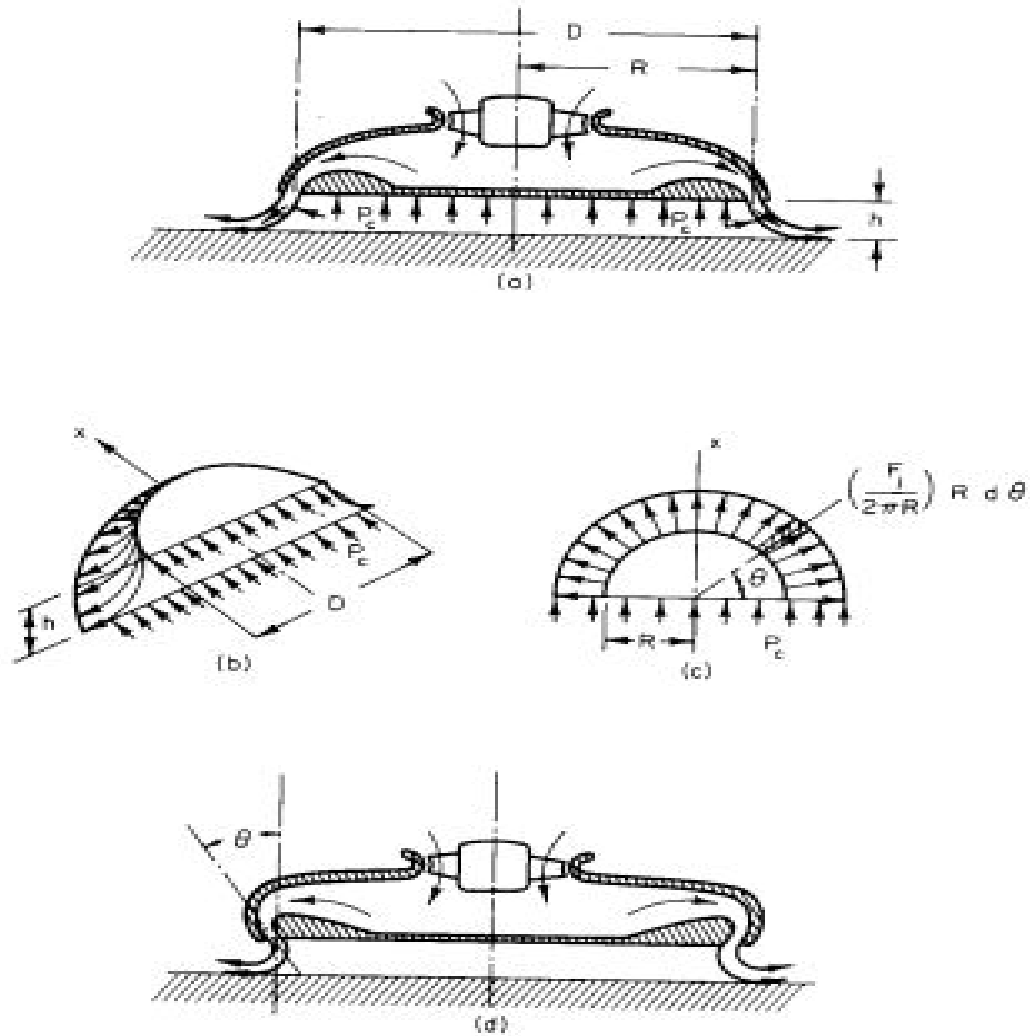


Figure 45. Flow in a peripheral-jet ground-effect-machine.

and below the machine and neglecting the incoming momentum of the air, the weight that the jet system in ground effect can support is obviously

$$W = F_j + p_c \frac{\pi D^2}{4}. \quad (12-3)$$

Out of ground effect, $W = W_\infty = F_j$. The ratio of W to W_∞ is referred to as the thrust augmentation factor A and from (12-2) and (12-3) becomes

$$A = 1 + \left[4 \frac{h}{D} + (8 - 2\pi) \left(\frac{h}{D} \right)^2 \right]^{-1}. \quad (12-4)$$

The same procedure can be followed for other cases than that in which the jet issues vertically downward. It can be advantageous to incline the jets inward through some angle θ , as shown in Fig. 45. However, there is little to be gained in going through the algebraic exercise of deriving A for the general case, Instead, the augmentation factor is taken from Ref. 2.

$$A = \cos \theta + \left[\frac{1 + \sin \theta}{4 \left(\frac{h}{D} \right) + 4 \left(\frac{h}{D} \right)^2 \left(\frac{2 \cos \theta + \cos \theta \sin \theta - \frac{\pi}{2} - \theta}{(1 + \sin \theta)^2} \right)} \right] \quad (12-5)$$

Equation (12-5) is presented graphically in Fig. 12-3 with some unpublished data for the particular case of $\theta = 0$. Although not too obvious

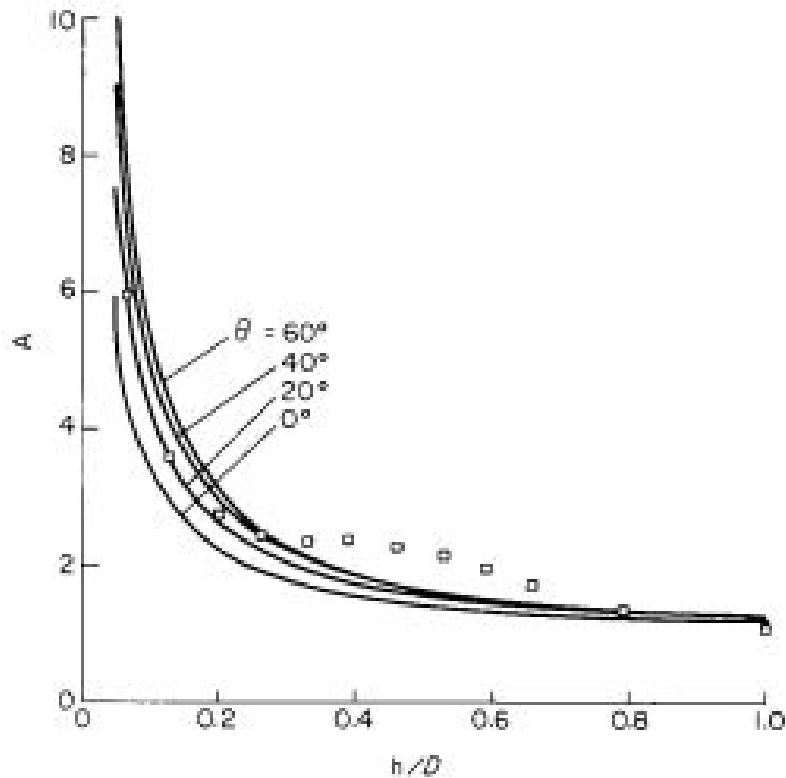


Figure 46. Thrust augmentation ratio versus height – diameter ratio: ----- theory [Eq. (12-5)];
 \square = unpublished data, $\theta = 0^\circ$.

from the illustration, the optimum θ for maximum A increases as h/D decreases. As h/D approaches zero, the optimum θ approaches 90° . The nearly constant experimental values of A between h/D -values of 0.25 to 0.5 are typical of other experimental results.

Next consider the power required by a peripheral jet GEM to hover. If t is the thickness of the jet and v_j , the jet velocity, the power delivered to the jet is

$$P = Q \Delta p \\ = (\pi D t v_j) \frac{1}{2} \rho v_j^2.$$

The actual power required will depend on the losses in the internal ducting and the efficiency of the fan. If they are combined into a single efficiency, η , then the required horsepower can be expressed as

$$\text{hp} = \frac{\pi D t \rho v_j^3}{1100 \eta} \quad (12-6)$$

The total flux of jet momentum F_j can be written as

$$F_j = \pi D t \rho v_j^2 \quad (12-7)$$

The total lift of the machine W is thus $A F_j$ or

$$W = A \pi D t \rho v_j^2.$$

Hence the lift per horsepower is

$$\begin{aligned} \frac{W}{\text{hp}} &= \frac{1100 \eta A}{v_j} \\ &= \frac{2200 \eta \sqrt{\rho} \sqrt{t/D} A^{3/2}}{\sqrt{W/S}} \text{ lb/hp}, \end{aligned} \quad (12-8)$$

where W/S is the weight loading with S equal to $\pi D^2/4$, Hence all other factors being equal the power loading increases inversely with the square root of the weight loading. The identical result was obtained for a propeller operating at zero forward speed. From Eq. (4-16) for a propeller

$$\frac{T}{\text{hp}} = \frac{550 \sqrt{2\rho}}{\sqrt{T/S}} \text{ lb/hp.} \quad (12-9)$$

These power and thrust relationships can be expected to hold only where the thickness of the jet is small in comparison with the height and diameter. Generally speaking, the predictions are optimistic in comparison with experimental data, at least as far as the power is concerned. Figure 47 compares model data taken from Ref. 3 with calculations based on Eqs. (12-4) and (12-8) from which the experimental values of pounds per horsepower for h/D values of 0.12 and 0.06 are seen to be significantly lower than the theory would predict. The experimental values, however, are still well above the value of pounds per horsepower for the ideal statically thrusting propeller with a disk loading of 20 psf.

Figure 48 presents the results of calculations based on Eqs. (12-5) and (12-8) for a range of h/D -, θ -, and W/S -values for a constant value of t/D of 0.08. The selection of the combination of these design parameters depends on other factors in addition to the aerodynamics. For example, the minimum value of h that can be tolerated will depend on the maximum obstacle height one wishes to pass over. From a power standpoint, of course, the lower the h and W/S the better. Generalized design studies tend to indicate that the place of the GEM in future transportation will probably be as large, high-speed ocean-going craft.

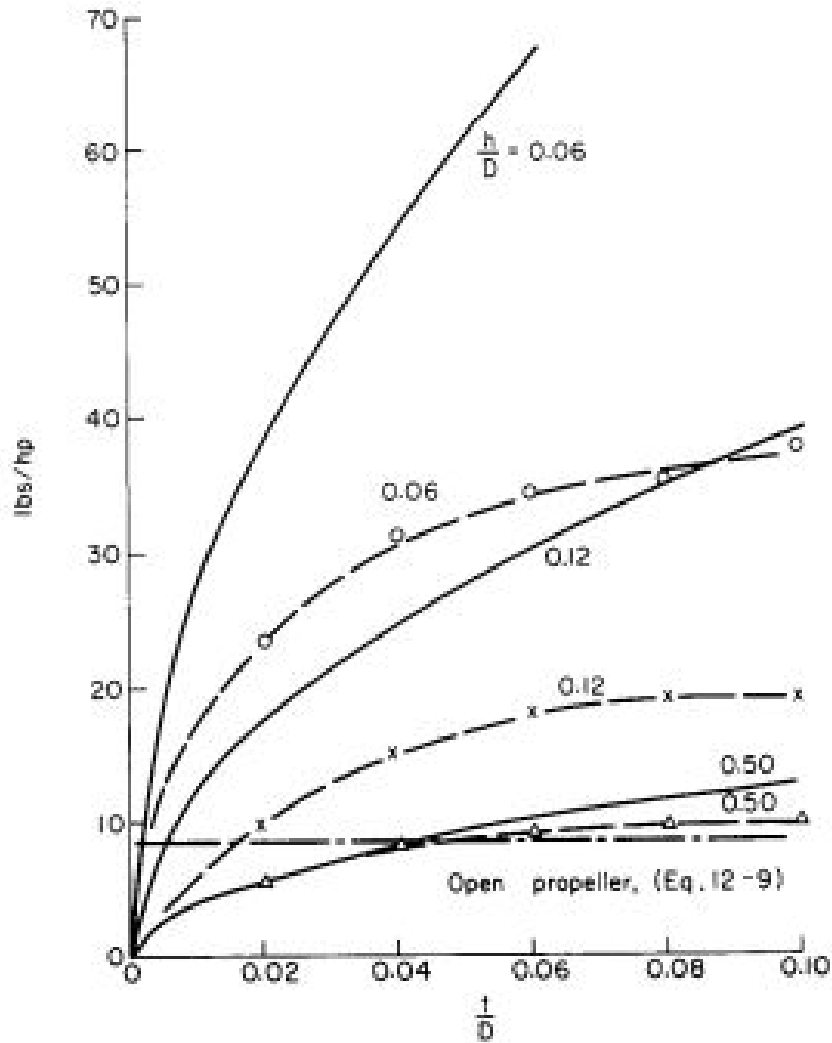


Figure 47. Lifting capability of GEM's: - - - experimental (Ref.3), _____theory[Eq. 12-8]; W/S = 20 psf; hp = jet horsepower.

Presently, machines are operating commercially with gross weights of approximately 30 tons up to speeds of 80 mph with an installed horsepower of 4000. Larger machines up to 100 tons with speeds of 120 knots and power of 10,000 hp are currently in the design stage. The weight loadings of these machines are fairly low at about 10 psf of base area. The power loadings are approximately 16 to 20 lb/h nearly double that of helicopters.

The GEM in Forward Flight

In forward flight power must be supplied to overcome the drag of the GEM in addition to sustaining the weight of the machine. Although the

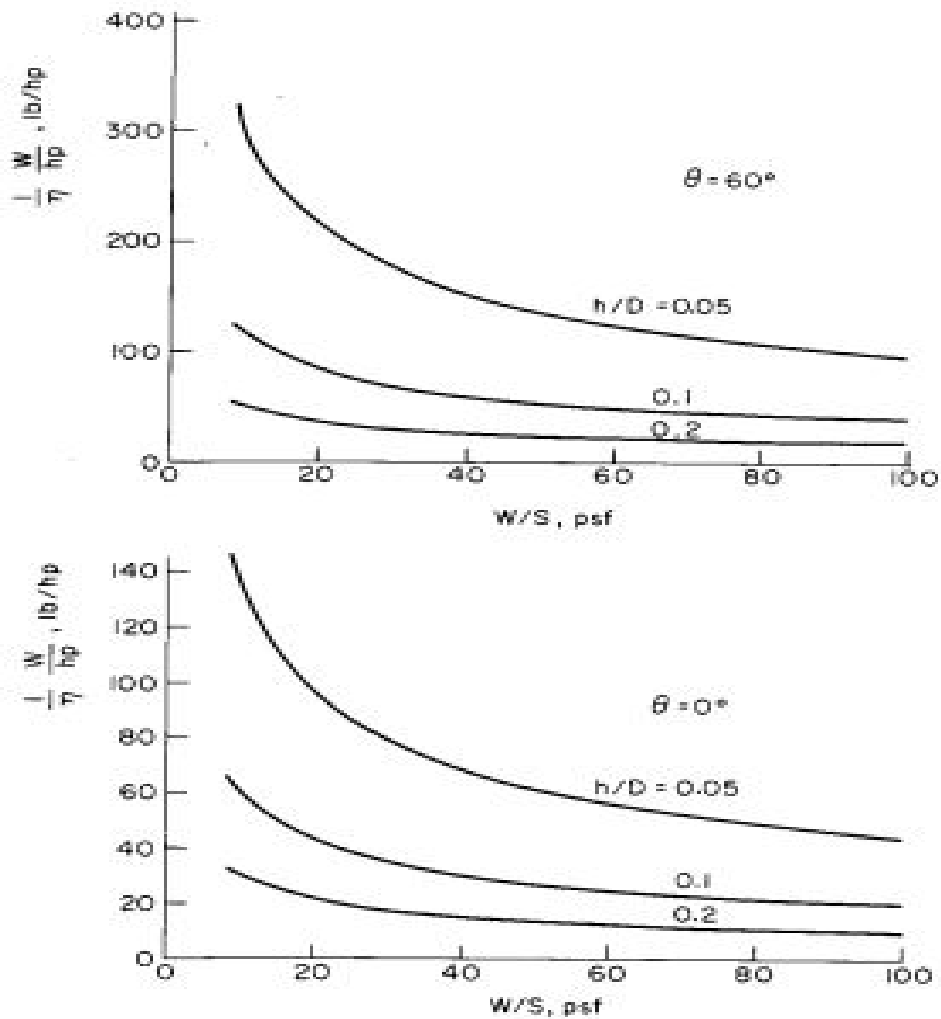


Figure 48: Effect of height, disk loading, and jet angle on power loading

available data are somewhat conflicting, there is evidence that the thrust augmentation factor does not vary radically with forward speed. Thus the power required in forward flight is approximately equal to the sum of the power calculated to hover and the product of the drag and the forward speed. The drag is equal to the sum of the parasite drag and the momentum drag. Hence it is important for an economically feasible, high-speed GEM to be aerodynamically clean.

The momentum drag is not so high as one might think. If M_j is the mass flux through the machine, the momentum drag might be calculated as the product of the forward speed and M_j . However, experimental data suggest a thrust recovery of this momentum somewhat similar to the jet flap. What little data are available in this regard show the momentum drag to be approximately half of the product of V and M_j .

The effect of forward speed on the lift augmentation factor is presented in Fig. 49, taken from the work of Higgins and Martin reported in Ref. 4. We cannot really generalize on these curves because the results must depend

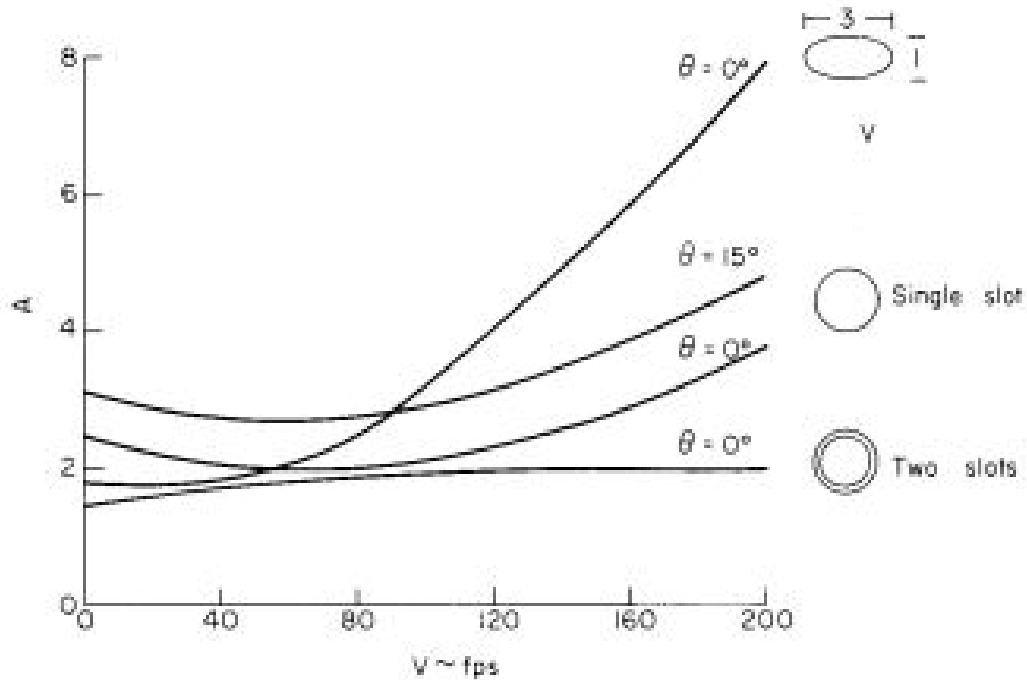


Figure 49. Effect of forward speed on augmentation ratio: $D = 16$ in., $h/D = 0.1$, all slots 0.06 in.; elliptic planform has same base area as circular planforms.

on the height of the machine above the ground, the ratio of jet velocity to forward speed, and the external shape of the machine. However, these data, as well as those obtained by others, show no serious deterioration of A with forward speed and even suggest the possibility of some increase of A with V .

Operation of a GEM over Water

The operation of a **GEM** over water is similar to that over a solid surface with some small exceptions. At low forward speeds the higher base pressure displaces the water downward relative to the undisturbed surface. However, Eq. (12-5) still holds if h is measured in relation to the displaced surface. The magnitude of this displacement is, of course, equal to the base pressure expressed in inches or feet of water.

At low forward speeds, therefore, the **GEM** over water behaves like a displacement vessel. This means that in addition to the other sources of drag we must add a wave drag. As the velocity increases, a point is reached at which the displacement of the water surface is negligible. This results since the impulse applied to each fluid particle by the base pressure becomes less and less as the speed increases. This behavior is illustrated in Fig. 50. Here a drag breakdown is shown for the **S.R.N. 1**, an 85%-lb machine with 535 ft² of base area. For this particular craft the wave drag reaches a maximum at about 12 knots.

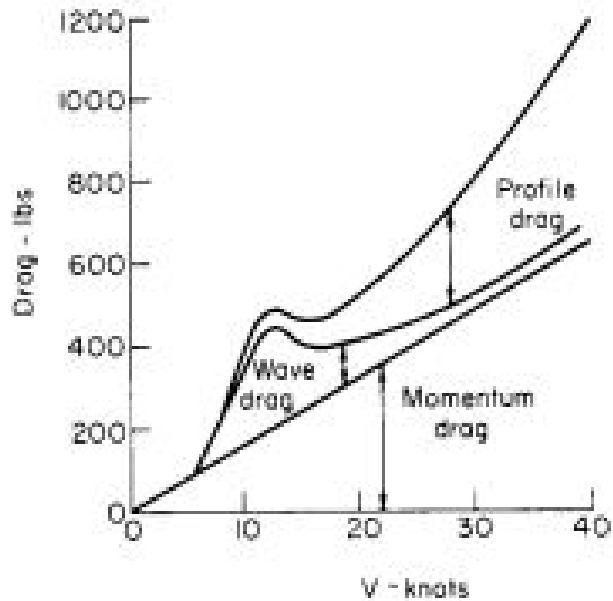


Figure 50. Drag breakdown of a GEM; $W = 8500 \text{ lb}$, $S = 535 \text{ ft}^2$.

Static Stability and Control of a GEM

One of the problems of a GEM is its marginal inherent handling quality. A pure peripheral jet exhibits a slight stability in pitch at very low heights. However, this stability deteriorates rapidly as the height is increased above

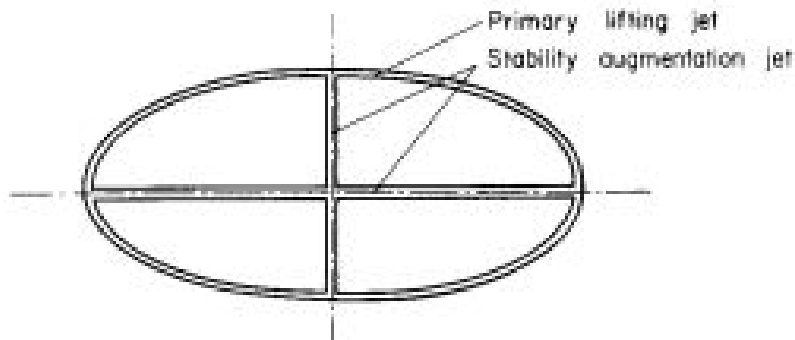


Figure 51. Subdivision of GEM base to improve stability.

approximately 10% of the diameter. The GEM is inherently stable in heave; that is, as the height tends to increase, the decreasing lift drops the machine back to its trimmed height. Obviously, if we attached several small machines together at the end of a boom, the result would be stable both in heave and pitch. This is essentially the scheme by which the pitch stability of GEM's is improved. Additional slots are cut in the base to divide the machine effectively into a number of smaller machines capable of sustaining different pressures under different portions of the base. Such a method is shown schematically in Fig. 51. The effect of subdivision of the base on the slope of the pitching moment curve with α is shown in Fig. 52. Here a stability slot has been installed along the x-axis only. Hence the stability is affected only about the x-axis. The result is a greater height for neutral stability about the x-axis than the y-axis.

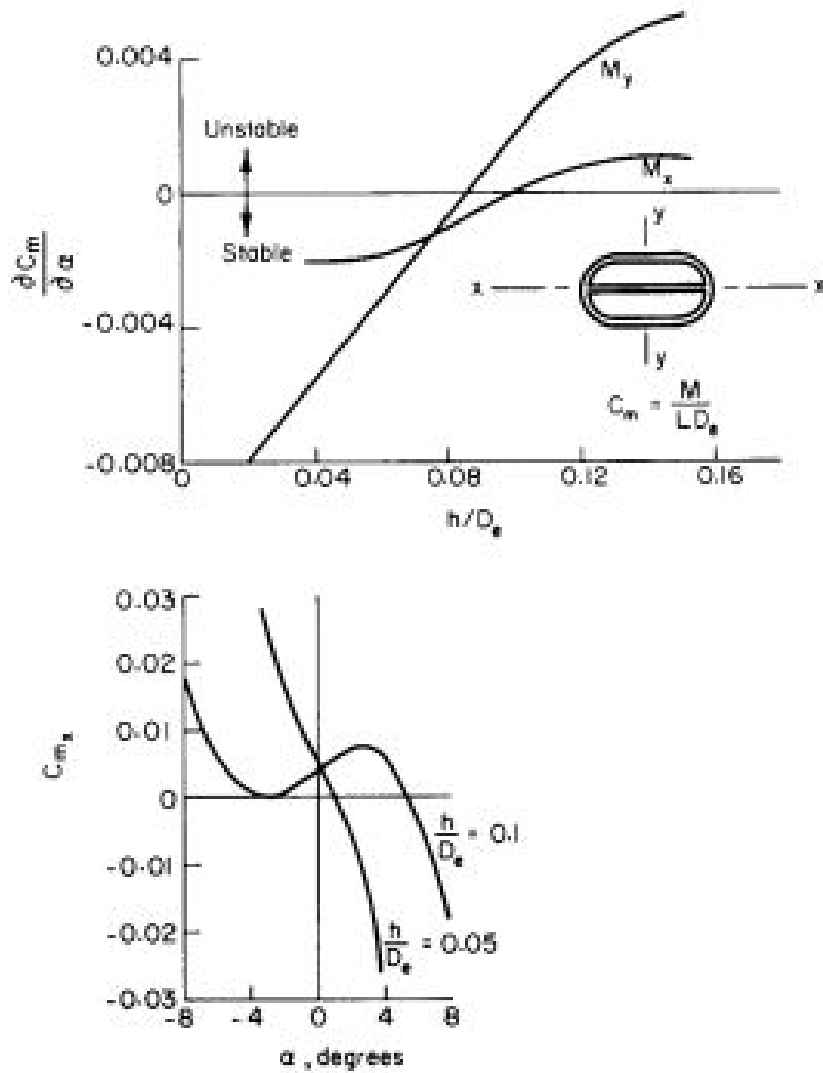


Figure 52. Effect of stability slot on static pitching moments; M = moment; L = lift; D_e = equivalent diameter; $D_e^2/4$ = base area.

This improvement in stability is not obtained free, however. Figure 52 shows the decrease in A as the result of adding inside slots.

Another somewhat similar scheme for improving the stability of a **GEM** is presented in Ref. S. An inside jet is incorporated to parallel the outer jet, as shown in Fig. 53. According to the reference, the normal distance between the two slots should be twice the height of the base above the ground in order to provide satisfactory stability. The control of **GEM**'s can be accomplished either by diverting some of the air applied to the base or by providing sources of separate thrusts such as external propellers. The second scheme seems to be gaining favor, as the control forces available with the base air are somewhat limited. Variations include a steerable propeller, ducted or open, and a fixed-propeller with movable control surfaces in its slipstream.

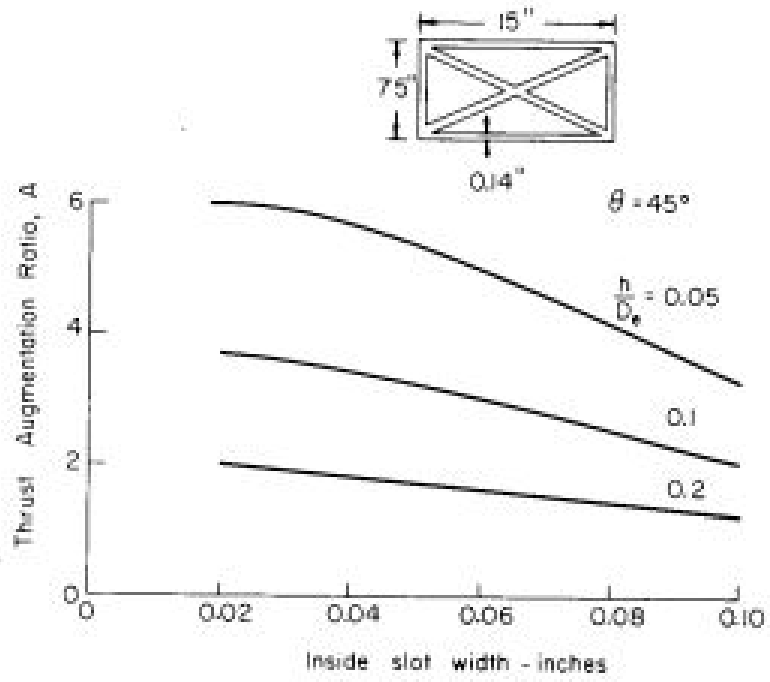


Figure 52: Effect of stability slots on thrust augmentation ration.

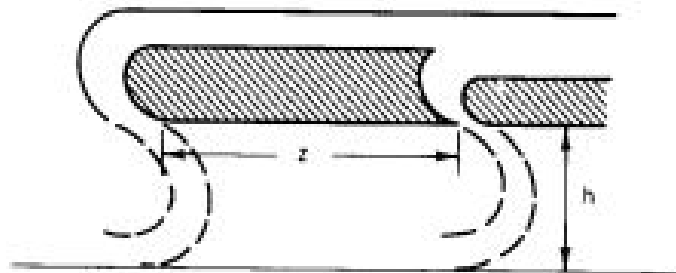


Figure 53. Stability augmentation system for GEM